[redacted]

HIGH REPETITION RATE SWITCH DEVELOPMENT

Robin J. Harvey

Hughes Research Laboratories
3011 Malibu Canyon Road
Malibu, CA 90265

April 1982

N60921-80-C-A290

Final Report

For Period 19 August 1980 through 20 March 1981

Approved for public release; distribution unlimited

Sponsored By
DEFENSE ADVANCED RESEARCH PROJECTS AGENCY (DoD)
Arlington, VA 22209

Monitored By
Dr. Frank M. Rose
Naval Surface Weapons Center
Dahlgren, VA 22448

[redacted]
SECTOR TECHNOLOGY

UNCLASSIFIED

SECURITY CLASSIFICATION OF THIS PAGE (When Data Entered)

REPORT DOCUMENTATION PAGE		READ INSTRUCTIONS BEFORE COMPLETING FORM
1. REPORT NUMBER	2. GOVT ACCESSION NO.	3. RECIPIENT'S CATALOG NUMBER
4. TITLE (and Subtitle) HIGH REPETITION RATE SWITCH DEVELOPMENT		5. TYPE OF REPORT & PERIOD COVERED Final Report 19 Aug 80 - 20 Mar 81 6. PERFORMING ORG. REPORT NUMBER
7. AUTHOR(s) Robin J. Harvey		8. CONTRACT OR GRANT NUMBER(s) N60921-80-C-A290
9. PERFORMING ORGANIZATION NAME AND ADDRESS Hughes Research Laboratories 3011 Malibu Canyon Road Malibu, California 90265		10. PROGRAM ELEMENT, PROJECT, TASK AREA & WORK UNIT NUMBERS
11. CONTROLLING OFFICE NAME AND ADDRESS Defense Advanced Research Project Agency Arlington, Virginia 22209		12. REPORT DATE April 1982 13. NUMBER OF PAGES 53
14. MONITORING AGENCY NAME & ADDRESS(if different from Controlling Office) Dr. Frank M. Rose, F12 Naval Surface Weapons Center Dahlgren, VA 22448		15. SECURITY CLASS. (of this report) UNCLASSIFIED 15a. DECLASSIFICATION DOWNGRADING SCHEDULE

16. DISTRIBUTION STATEMENT (of this Report)

Approved for public release; distribution unlimited.

17. DISTRIBUTION STATEMENT (of the abstract entered in Block 20, if different from Report)

18. SUPPLEMENTARY NOTES

19. KEY WORDS (Continue on reverse side if necessary and identify by block number)

High power, Crossatron switch, high repetition rate, closing switch

20. ABSTRACT (Continue on reverse side if necessary and identify by block number)

The Crossatron switch is a hybrid low pressure gas discharge device capable of operation at high frequency. Tests of a 38-cm-diameter Crossatron switch have been made with source currents up to 1 kA and anode voltages to 40 kV. The switch is shown to close in two phases. In the first phase the anode current rises abruptly ($\lesssim$10 ns) to a space charge limited level set by the area, the spacings, and the

DD FORM 1 JAN 73 1473 EDITION OF 1 NOV 65 IS OBSOLETE

UNCLASSIFIED

SECURITY CLASSIFICATION OF THIS PAGE (When Data Entered)

voltage. (As with vacuum triodes, this electron current can saturate if the source current is too low; it can also be controlled electrostatically using the control grid.) In the second phase, the current rise is exponential, starting from the space charge limit. The exponential growth rate scales linearly with both pressure and source current density and inversely with the short circuited anode current. The source current density is presently limited to 1-3 A/cm^2. In order to operate at high anode currents, with short (<50 ns) closure times, the source current density must be increased an order of magnitude. The empirical data predict that the time to reach full closure at 250 kV is about 23 ns when the source current exceeds the anode current at low operating pressure (35 mTorr He).

TABLE OF CONTENTS

LIST OF ILLUSTRATIONS

FIGURES PAGE

LIST OF DEFINITIONS

V_A	Anode Voltage
V_{CG}	Control Grid Voltage
V_S	Source Grid Voltage
I_A	Anode Current
I_{CG}	Control Grid Current
I_S	Source Grid Current
I_L	Load Current
A_o	Area of One Cathode Section
SG	Source Grid
CG	Control Grid
$R_{1/2}$	Line Impedance seen by switch (5 Ω)
R_L	2 $R_{1/2}$, Load Resistance (10 Ω)
K_1	Upper Cathode
K_2	Lower Cathode
Γ	Exponential Growth Rate
I_o	Maximum Short Circuit Switch Current ($V_o/R_{1/2}$)
V_o	Initial Anode Voltage
I_1	Space Charge Limited Current
BL	Blumlein Circuit
d	Anode to CG Separation
k	Child's Law Constant (2.33×10^{-6} A $V^{-3/2}$)

SECTION 1

INTRODUCTION AND SUMMARY

The Crossatron switch is a hybrid low pressure gas discharge device suitable for high frequency operation. It uses a plasma generated by a crossed-field discharge as a source of charge carriers and is grid controlled. The coaxial electrode structures are shown schematically in Figure 1. They include: an anode, a cathode, a source grid and a control grid. A dc magnetic field (localized to the gap between the source grid and the cathode) is used to sustain the source plasma when the source grid is energized. The source plasma can be formed at a voltage drop of ~250 V and is an adjustable source of charges analogous to a thermionic emitter but with a negligible thermal inertia. The anode current is initially controlled by the control grid potential. This provides for exceptionally short response times and high repetition rate operation.

The objective of this program was to demonstrate the basic operating mechanisms and project the ultimate physical limitations of the Hughes Crossatron switch for high repetition rate and high power operation. This work included theoretical and experimental analyses of the Crossatron. The long-range goals are reliable burst operation at 10 kHz, 60 kA, and 300 kV with 50 ns pulses rising in 3 ns. The evaluation was to be performed in the following four tasks:

1. Theory — calculate and compare theoretical models with experimental results.

2. Single Segment Model — test a crossatron model with a single cathode segment to 50 kV and >3 kA with a goal of <10 ns pulse rise time.

3. HV Bushing — test a bushing for 250 kV holdoff.

4. Synergistic Tests — test a segmented Crossatron switch to >6 kA in the burst mode at 150 kV.

A test model switch designed to meet the above goals is described in Section 2. An outer diameter of 40 cm was chosen in order to assure a source current glow-to-arc transition >3.5 kA with a safety factor of two to three.

Keywords: High Power Crossatron [illegible] high repetition rate [illegible] Switch, Electronic and electrical [illegible]

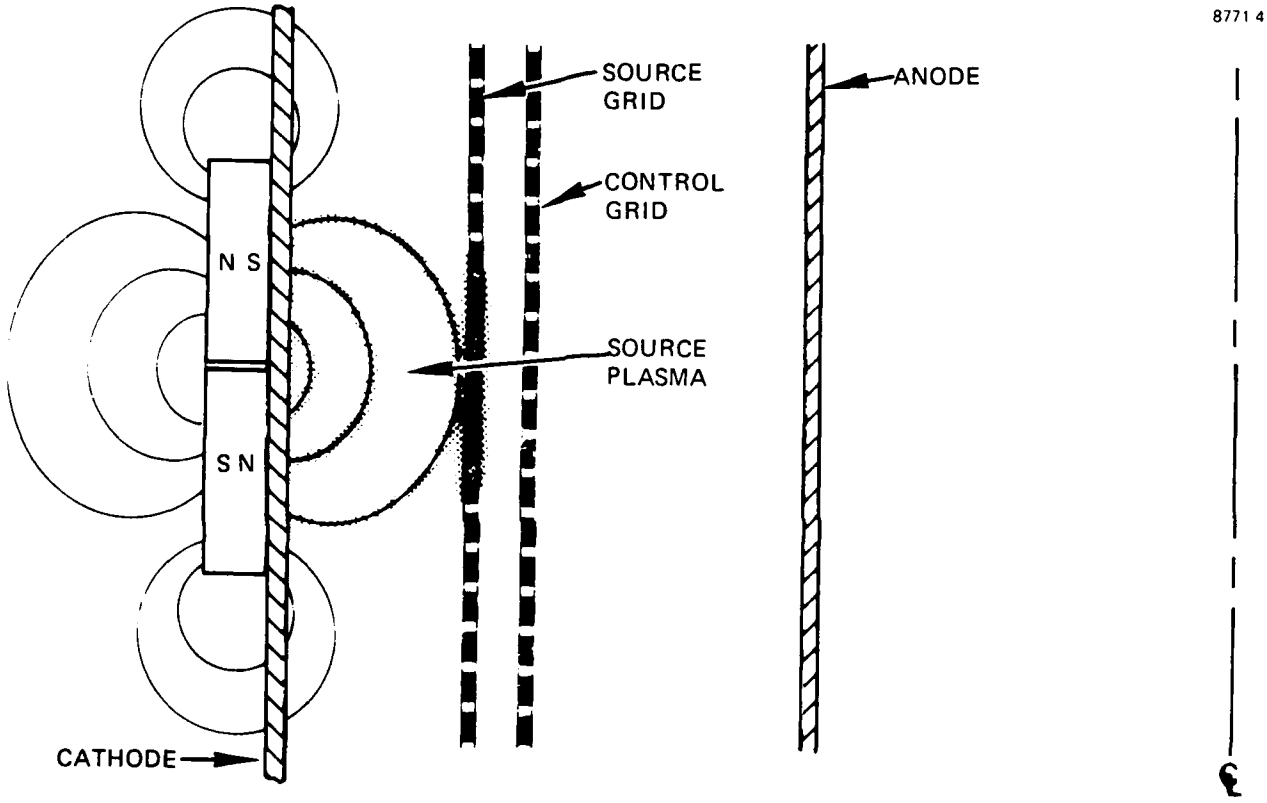

Figure 1. Crossatron switch electrode structure and source section schematic drawing.

The high voltage bushing and electrode designs are shown in Figure 2. The designs were aimed at protecting against vacuum flashover, while keeping the spacings as short as possible to prevent Paschen breakdown and providing a minimum transit time for charges to cross the 2-cm anode-to-control grid (CG) gap. Fiberglass insulators and O-ring seals were used in order to keep the design cost effective and demountable.

The experimental program included an examination of the basic parameters listed in Table 1. The switch behavior was found to be complex and full high power operation was never achieved. The high power testing of the completed switch is discussed in Section 3. These tests revealed a rapid (<10 ns) rise of current to a space-charge limited level followed by an exponential growth of current as illustrated in Figure 3. The growth rate Γ increases as a linear function of both the pressure P and the source current density J_S and decreases linearly with the short circuited anode current, I_o. The scaling of Γ with the source current, I_S, implies that in order to be effective as a fast closing switch I_S must exceed I_o.

An unanticipated factor in the testing was the unusually slow rate of conditioning of the electrodes to a high current density. As seen in Figure 4, the current carrying capability of the switch is far below that expected and is consistent with a contaminated vacuum surface. This has resulted in an ever increasing but still relatively low test current level of 2 kA at anode voltages to 40 kV. Parametric data have been obtained for the other important variables shown in Table I. Analyses of these data in Section 3 and 4 show that it is desriable to operate the switch with as high a source current density as possible. The switch connectors influence the response characteristics. As shown in Figure 5(a), the Blumlein (BL) should be connected between the anode and the cathode. With these connections, the anode current I_A provides a positive feedback to the control grid section. This feedback is not present when the BL is connected (see Figure 5(b)) between the anode and the control grid (CG). Instead, with this latter connection, the device behaves as a high frequency power amplifier.

Scaling of the space charge limited current and growth rate data results in a predicted switch closure time of about 23 ns at full power. Key to this behavior is obtaining a high source current density (10-20 A/cm^2) typical of that achievable with chemically clean electrodes. Proof of this would require sealing

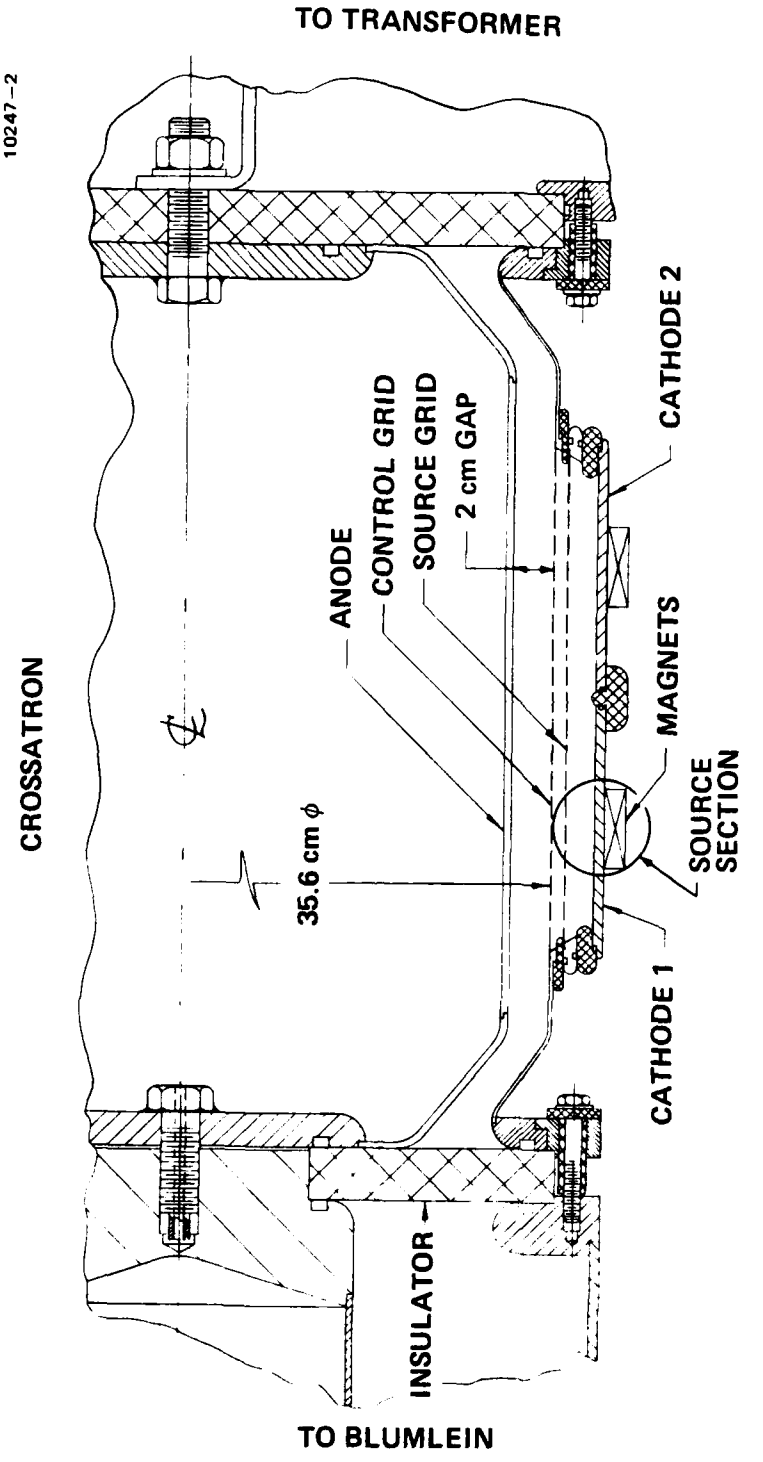

Figure 2. Crossatron design.

Table 1. Basic Parameters Examined

Parameter	Range
Pressure	0 to 100 mTorr He
Anode Voltage	0 to 40 kV
Anode Current	0 to 2 kA
Source Current	0 to 2 kA (0 to 1 kA each)
Control Grid { Bias Voltage	NA
Control Grid { Current	0 to 1.5 kA
Number of Source Sections	1 to 2
Connections to Blumlein	Anode to CG, Anode to SG
Relative Timing	Not specified
Conditioning Methods	Not specified
Anode Leakage Current	Not specified
Preionizer Timing	Not specified
Conduction Voltages	Not specified

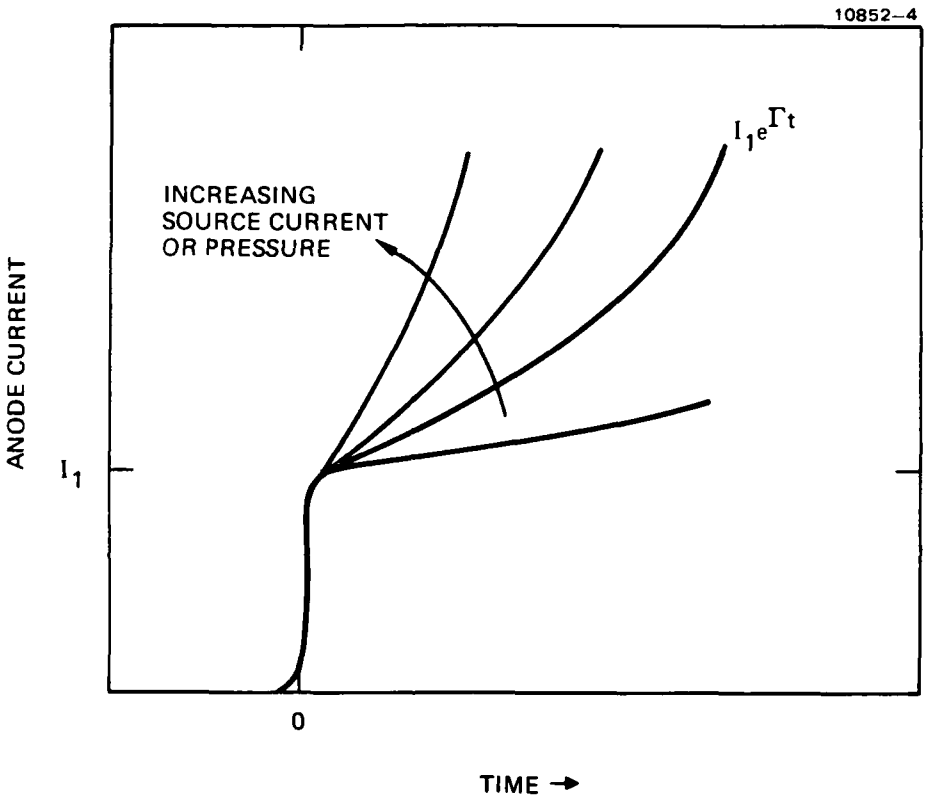

Figure 3. Characteristic switching behavior.

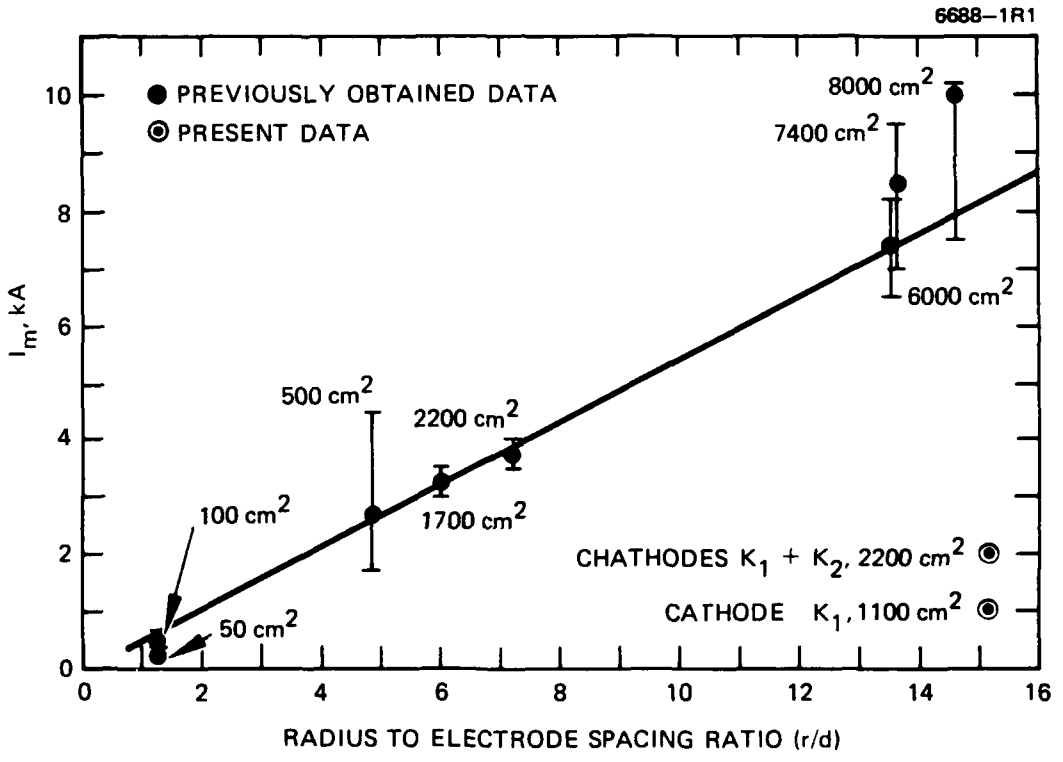

Figure 4. Empirical scaling of the maximum interruptible-current for HV-crossed-field interrupters as compared to the present source-current maximum at low voltage.

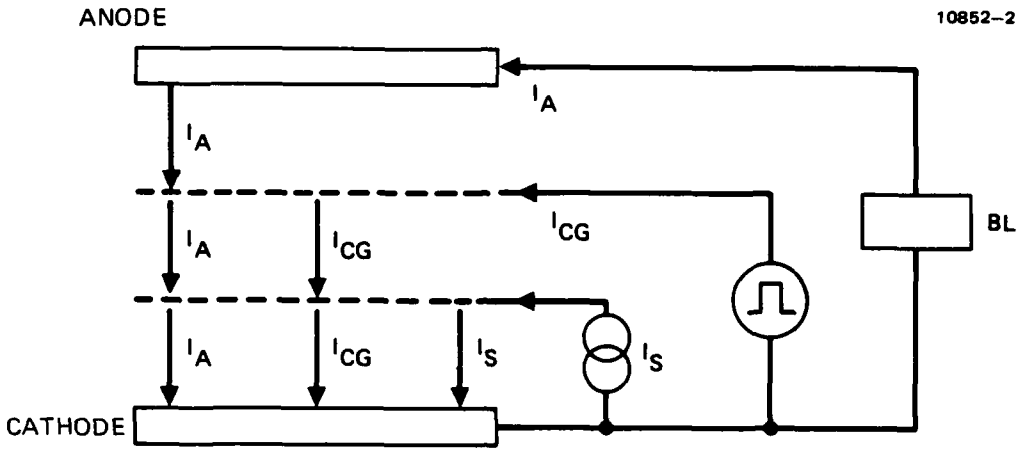

a) CLOSING SWITCH MODE WITH POSITIVE FEEDBACK THROUGH CONTROL GRID

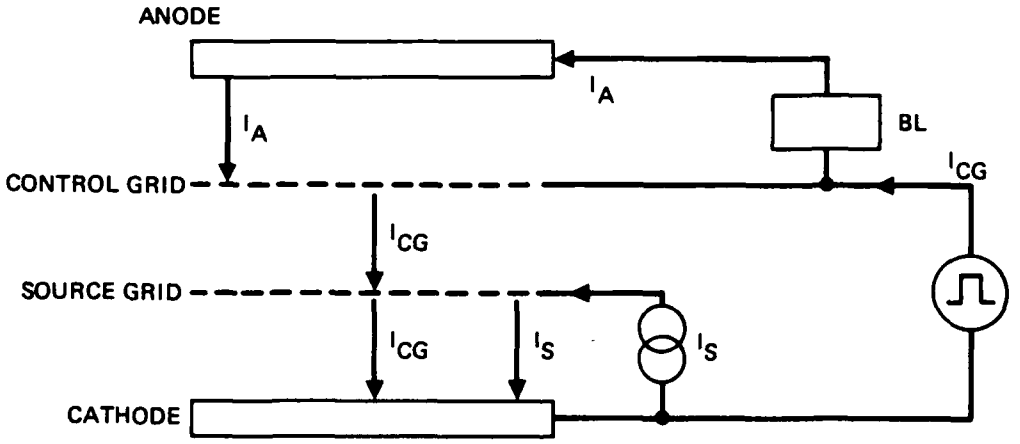

b) AMPLIFIER MODE WITH NO FEEDBACK BETWEEN CONTROL GRID AND SOURCE GRID

Figure 5. Effect of switch connection rearrangements. A third possible arrangement (with BL ground to source grid) was not attempted.

the surfaces of the fiberglass parts, electropolishing the cathodes, and chemical processing of the existing device prior to reassembly. Once the optimum configuration is established, conventional bakeable ceramic-to-metal seals should be employed.

SECTION 2

TEST MODEL FABRICATION

A. DESIGN AND FABRICATION

The Crossatron-test model design is shown in Figure 2. It uses fiberglass insulators and O-ring seals in order to be cost effective and demountable. Fabrication of the Crossatron was delayed due to difficulties with the control grid assembly shown in Figure 6. This assembly consists of stainless steel support rings at the insulators, spinnings connecting the support rings to adapter rings welded to the perforated grid structure. The cylinders ordered for the adapter proved to be out of round and remachining was needed following some design modifications.

Figure 7 shows the cathode assembly with the center fiberglass insulator ring. Figure 8 shows the source-grid assembly with its fiberglass vacuum seals and support rings on the ends. Fiberglass was also chosen for the main HV bushings because of its structural strength and low cost. While we had planned to seal the surface of the fiberglass, a suitable coating was not found in time and assembly proceeded without sealing.

B. TEST APPARATUS

1. Charging Circuit

The circuitry used for testing the Crossatron switch was modeled after that developed for the Experimental Test Accelerator at LLL.[2] A diagram of the circuit used to charge the Crossatron anode is shown in Figure 9. This circuit was fabricated in an oil barrel which also served as a support for the Crossatron switch. The components of this circuit are shown in the photograph of Figure 10. Mockup test results of this circuit at 250 kV and low repetition rates are shown in Figure 11. The oscillogram shows the charging transformer primary current and voltage in addition to the secondary voltage. The secondary voltage is the parameter of main interest. This voltage swings negatively and then positively to its peak value. Leakage currents in the Blumlein and switch typically reduce the level of the second peak relative to the first.

MC 13838

11837-12

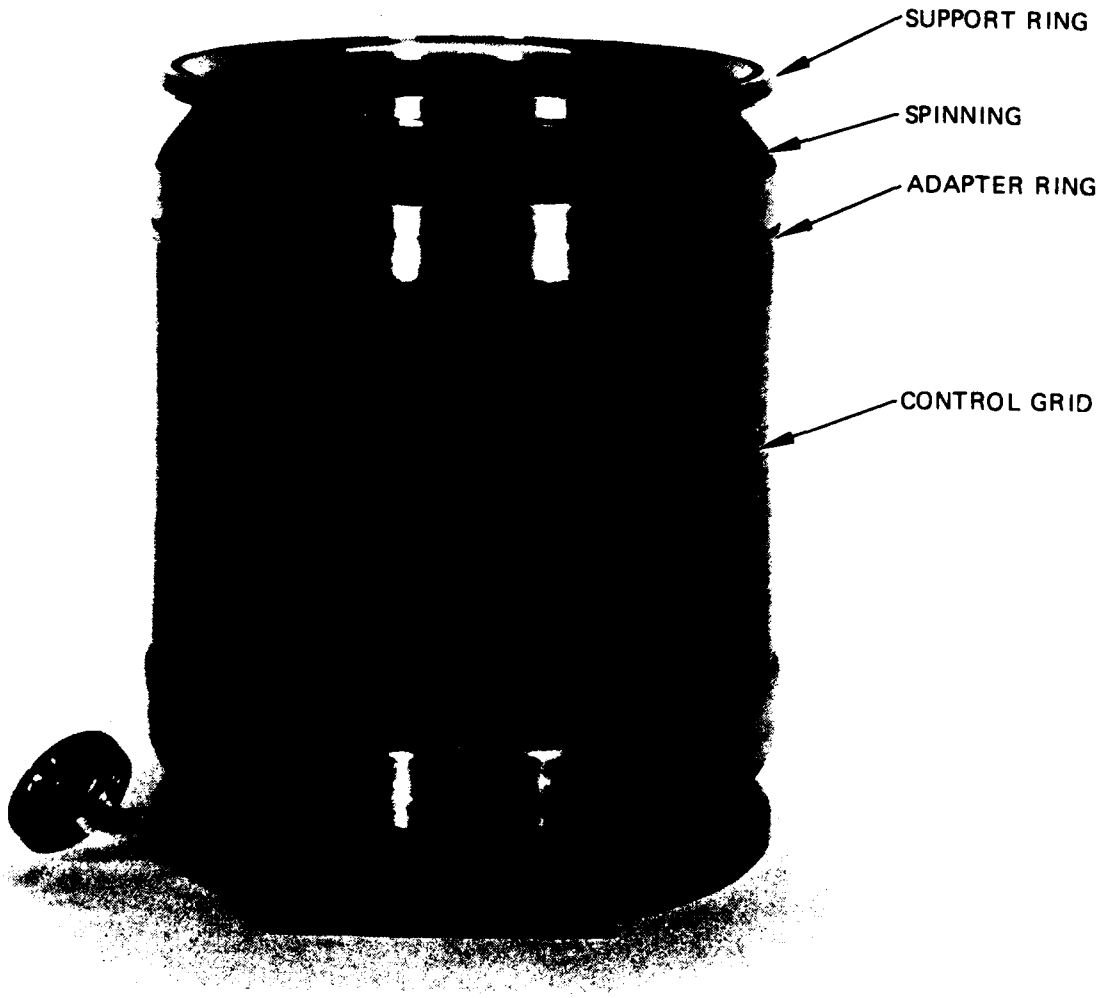

Figure 6. Control grid.

MC 13840

11837-14

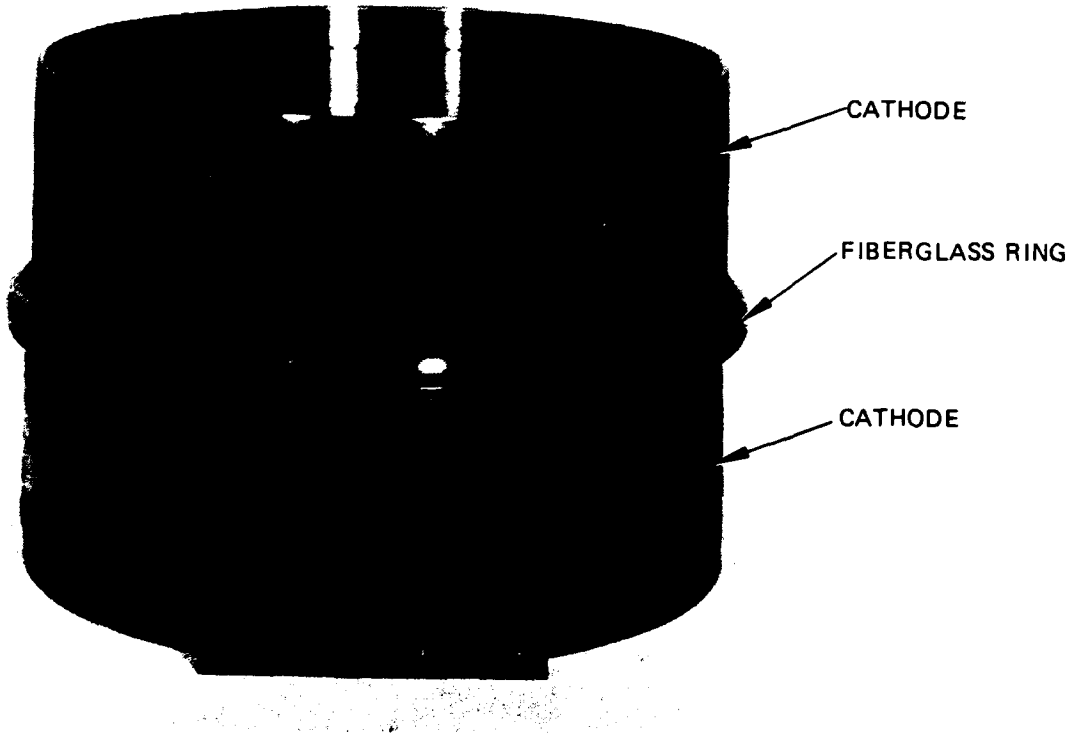

Figure 7. Cathode assembly.

11837-13

MC 13837

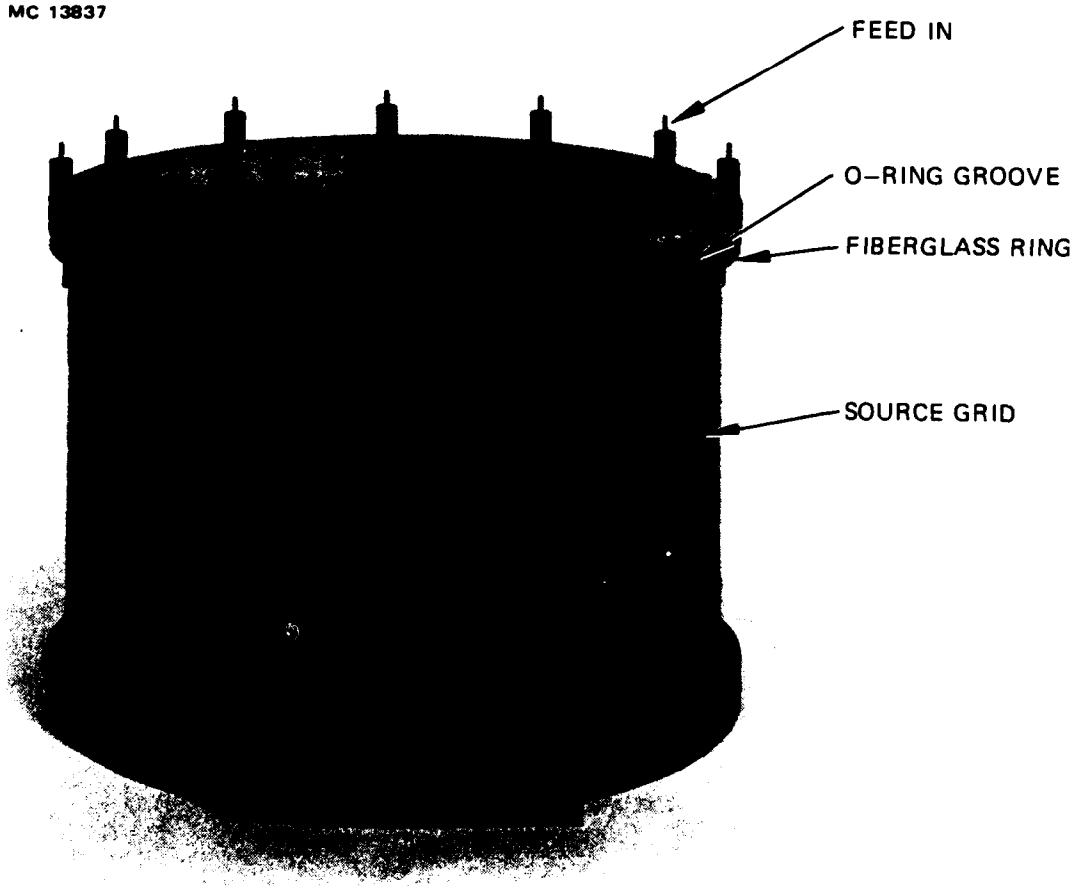

Figure 8. Source grid.

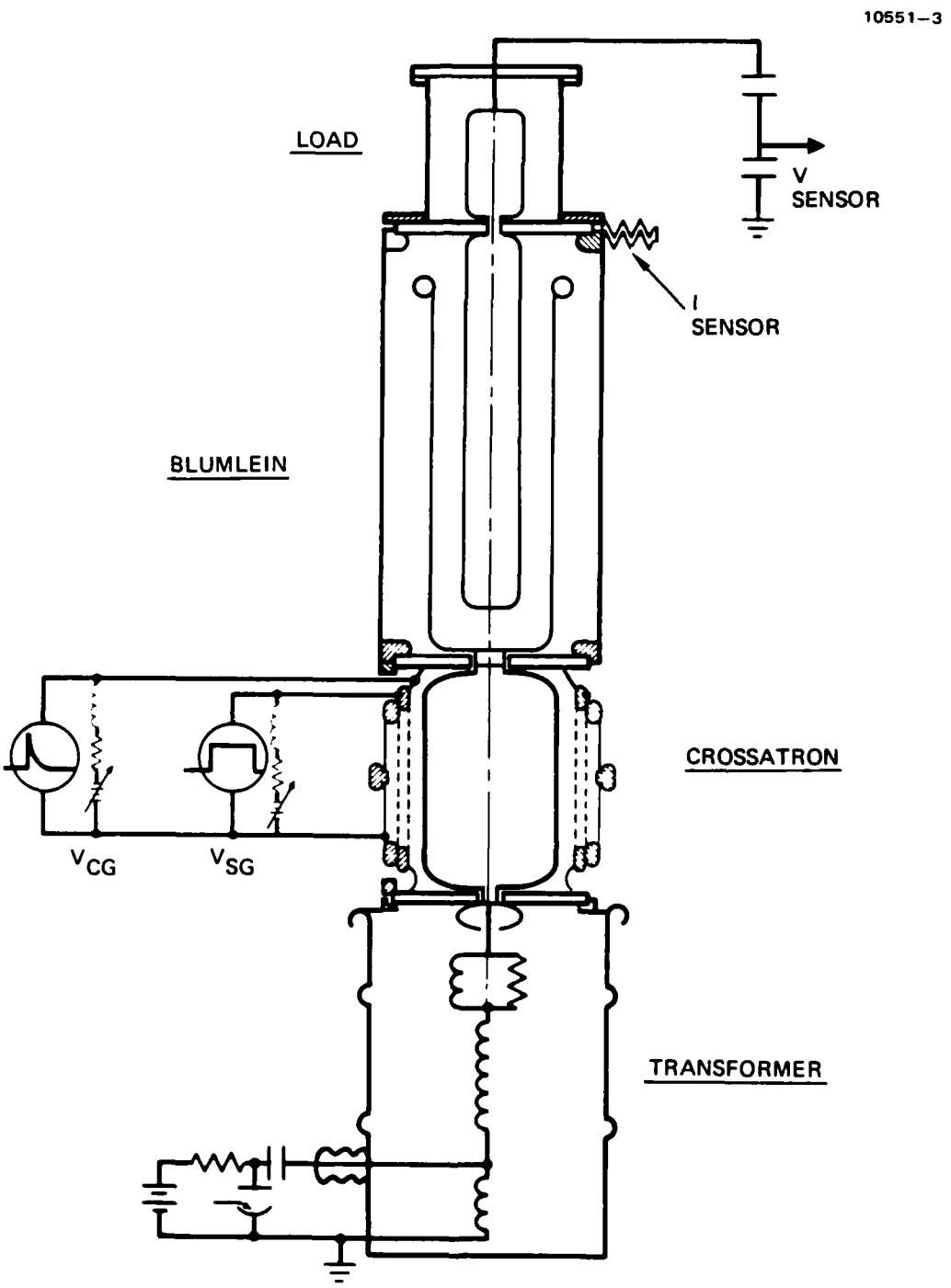

Figure 9. Crossatron test setup.

13806-21

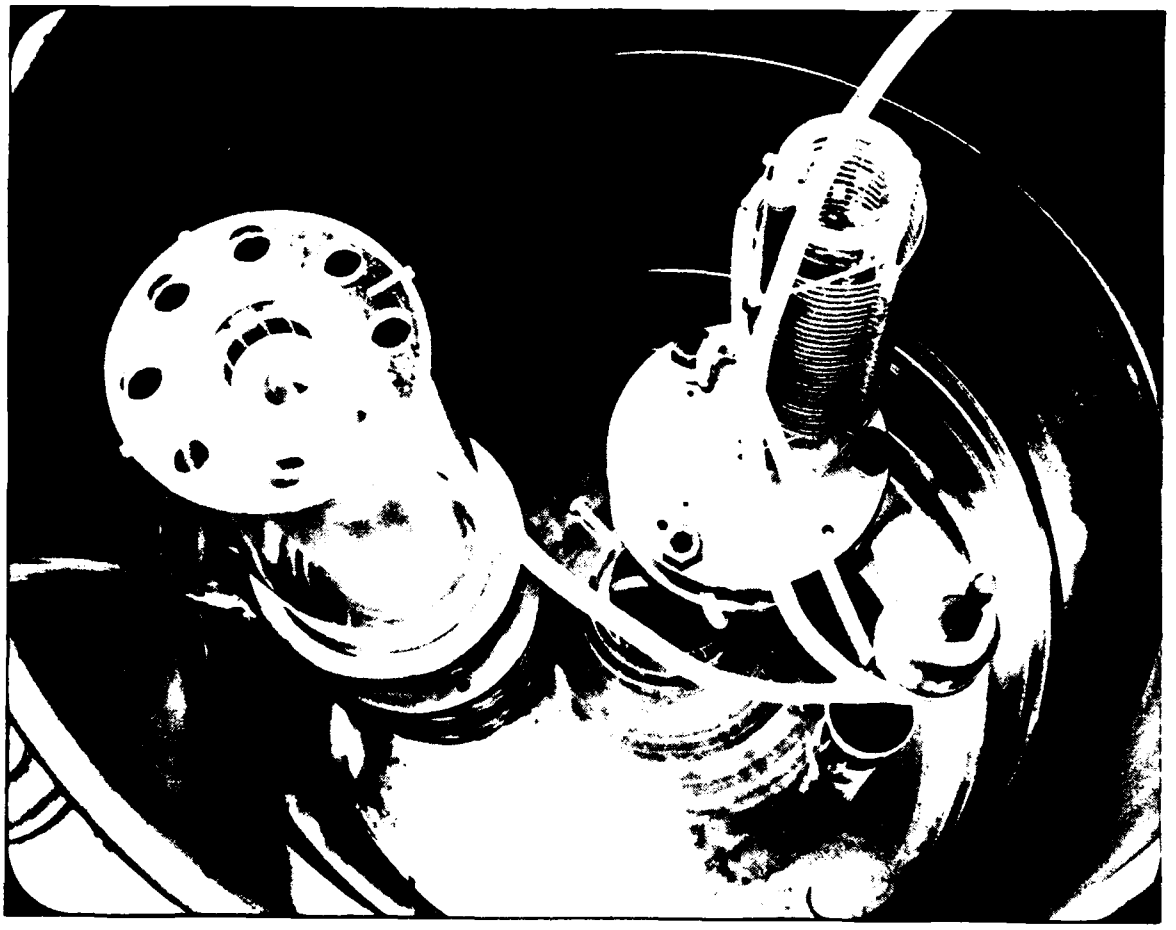

Figure 10. Components of the Anode Charging Circuit.

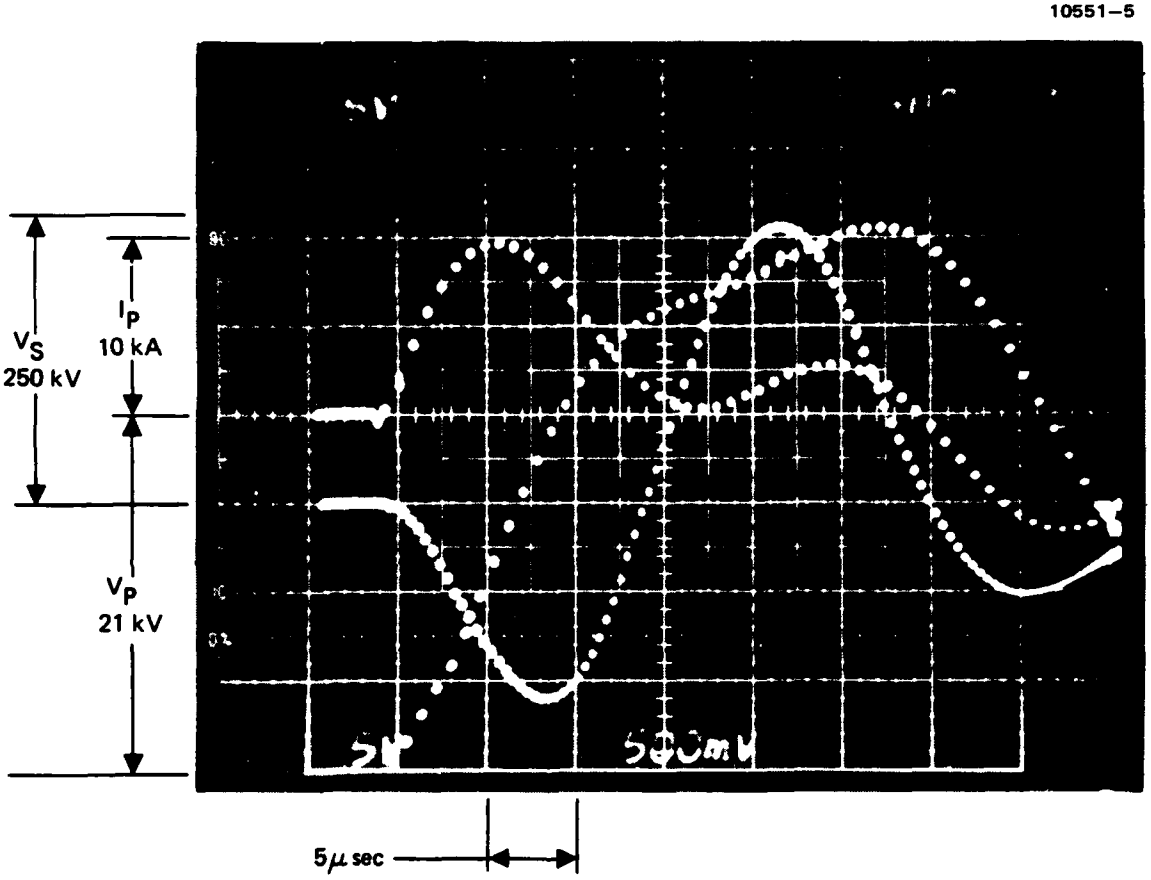

Figure 11. Pulse transformer test
V_S = 250 kV

2. Blumlein

A diagram of the water-insulated 10-Ω line is shown in Figure 9. This unit is assembled on top of the Crossatron. It serves as the storage capacitor for the charging circuit. (A water treatment system is used to obtain deionized water.) The switch sees a 5-Ω line with a period of about 50 ns.

3. Load

A 10-Ω Cu_2SO_4 (H_2O) load is assembled on top of the Blumlein as shown in Figure 9.

4. Pulsers

The pulser arrangement is shown in the simplified schematic of Figure 12. The source-grid pulser supplies ~30-μs wide pulses of up to 3 kA between each cathode segment and the source grid. The components are suitable for operation at 3.5-kA pulses spaced at 100 μs for a 10-kHz burst rate. A two-pulse unit has been assembled, but only run in single pulse mode. A Pulspak 10A Precision Pulse generator is used to drive the CG. This instrument has a 1-ns jitter for a 10-kV, 400-A short circuit output pulse.

5. Magnets

The magnetic field sustainer magnets were modeled after our previous designs. In this case we have chosen plastic strip magnets which are wound on the cathode walls.

6. Sensors

Current transformers are located at all of the inputs to the switch. A capacitive voltage divider is located in the transformer output stage. A high speed current shunt of our own design is installed in the Blumlein circuit load. The rise time of this shunt is less than 5 ns when used with our 7600 series storage oscilloscopes. While additional shunts were prepared in order to lower the system inductance, there has not been a need to complete that installation.

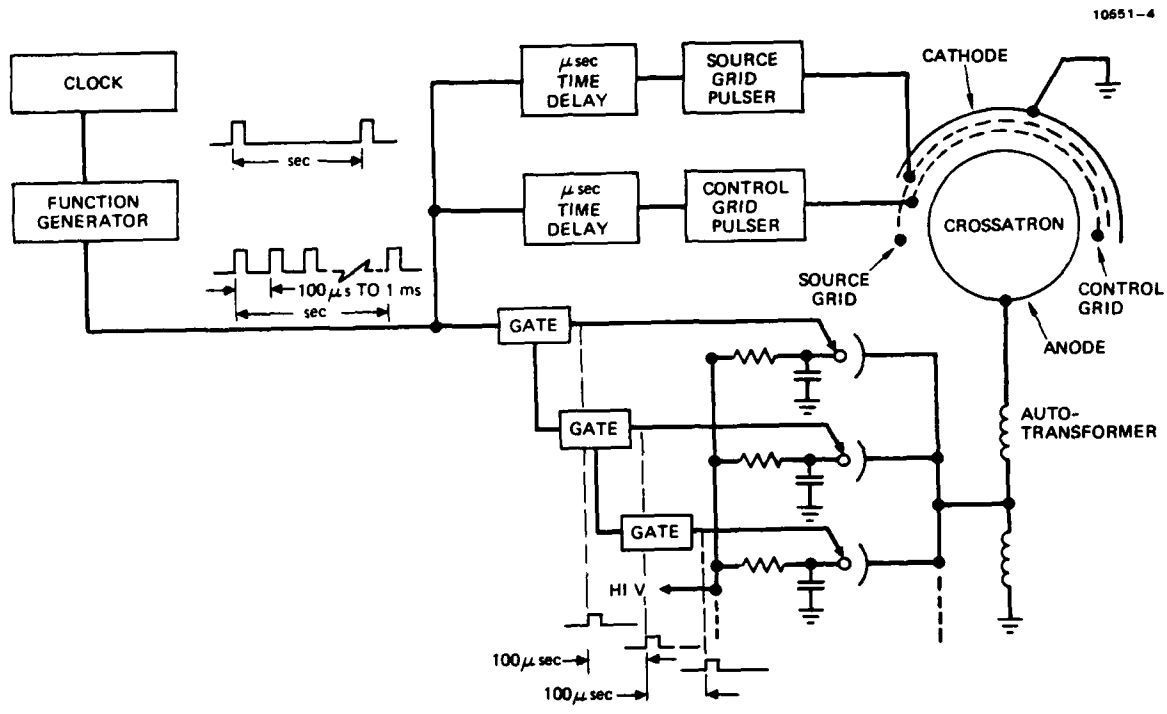

Figure 12. Crossatron test setup. (Pulse Burst).

7. Completed System

The completed switch and test assembly is shown in Figure 13. The load is at the top of the cylindrical BL. The cathode is shown connected electrically to the BL with metal straps. The magnet assemblies are visible on the outside of the two cathodes. The HV pulse transformer housing serves as the support for the system.

M13910

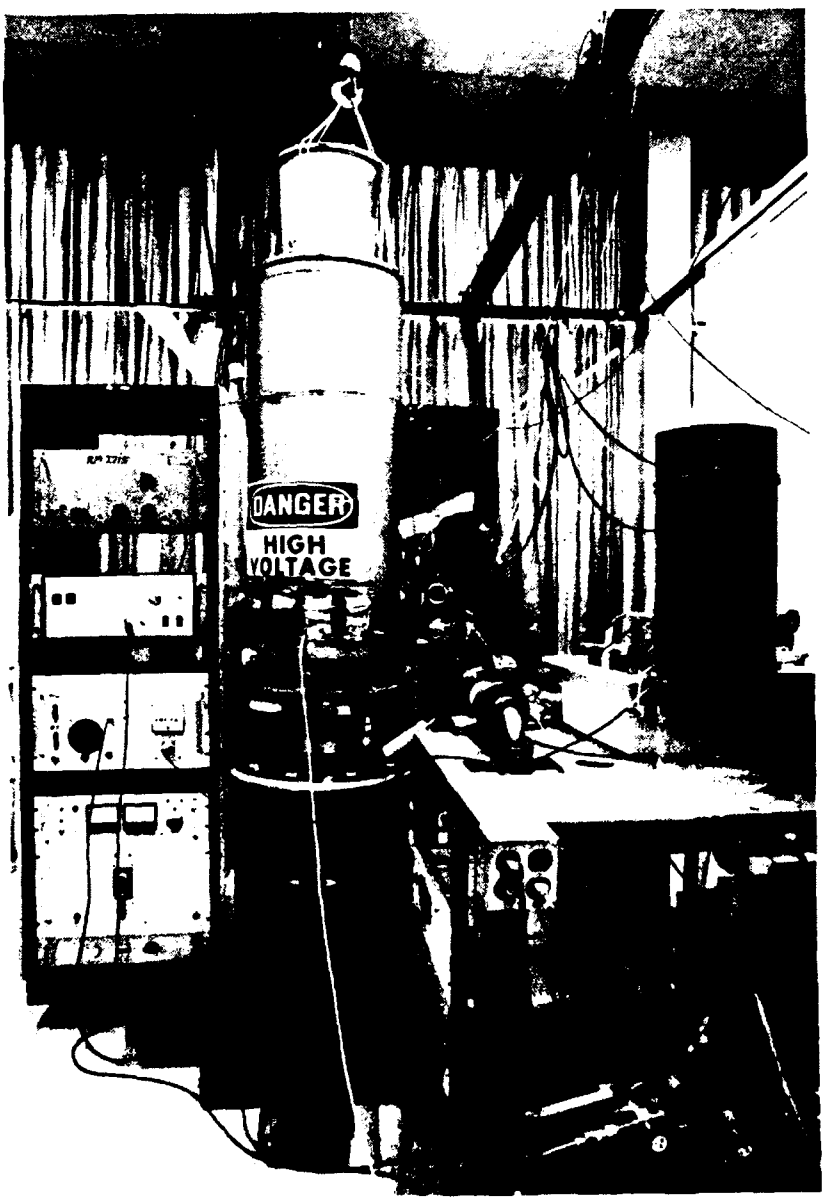

Figure 13. Completed switch system.

SECTION 3

EXPERIMENTAL SWITCH TESTS

The testing of the switch was originally planned to cover the measurement of the rise time of single pulses, followed by a demonstration of burst mode operation with more than one cathode section. The first electrical tests were made with the control grid (CG) grounded to the Blumlein. This arrangement had the lowest inductance and, based on earlier experiments with smaller switches, there was reason to expect a lower conduction voltage. It was quickly discovered that, while the anode current had a fast rise time, it was too low in amplitude and the switch would not fully close. A review of our earliest switch models showed a 1:1 current amplification with these connections, in agreement with the experiments. A lack of positive feedback into the CG section was correctly identified as the problem. Consequently, we rearranged the circuitry to force the anode current to flow past the control grid and into the rest of the switch. the first attempts at switching in this mode were also unsuccessful due to surface flashover at the (CG) mounting bolts. The transient control grid voltage (V_{CG}) was sufficient to modulate the anode current into a series of pulses, but was not high enough to get full conduction.

Once we corrected the CG arcing problem, we were able to obtain a full discharge of the anode voltage. A detailed analysis of the parametric behavior of the switch was begun as discussed in detail below. The range of this investigation was constrained to currents under a few kiloamperes due to arcing of the source current. This last major problem was not eliminated by extensive current conditioning. The effect of a low source current is to distort the anode current pulse shape. Scaling data were obtained in order to determine how this shape could be improved if the arcing problem were eliminated. These scaling data predict a total time to closure of 23 ns at full power. Below we sequentially consider the operation of each section of the switch.

A. SOURCE GRID SECTION

The source grid and the two cathodes (together with their magnets) consitute two independent cross-field discharge plasma sources. The surface area, A_o, of a cathode seciton is in excess of 1100 cm^2 while the active area covered by the magnets is 313 cm^2. Crossed-field interrupters[1] of these dimensions are normally expected to condition to over 8000 A in the interruption mode and much higher in the conduction mode (see Figure 4). The maximum level achieved with the present source sections is around 1 kA each due to glow-to-arc transitions. The glow-to-arc limitation is consistent with excessive contamination of the electrodes. Two arc types are evident. These are arcs between the SG and the cathode and between the SG and CG.

The SG-to-cathode arcs are gradually eliminated by normal operation and the source can be operated at over 1 kA without arcing to the cathode. Arcs to the CG are not eliminated by normal operation. Instead, the CG potential simply rises to that of the SG without drawing significant current and the anode is spontaneously switched on. Toward the end of the program, it was found that the CG surface would be conditioned by rearranging the circuit. The peak source-current conditioning level achieved by the end of the program was I_S ~2 kA.

The glow discharge conduction voltages in the source sections were found to average 370 V with a variance of about 50 V. This voltage drop increases with current and decreases with pressure. Figure 14 shows the upper section response at a pressure of 37 mTorr He. The discharge is preionized by a low current keep-alive circuit which breaks into oscillation at these low pressures and is seen in the random pattern of the voltage oscillation in the lower trace. Approximately 1250 V is switched across the electrodes and V_S rises momentarily to that level. The voltage then falls as the current grows; stabilizing after about 10 μs.

If excessive voltage is applied to the SG, its potential increases beyond that possible for crossed field conduction in the fixed magnetic field and the discharge extinguishes rather than grows. This is especially important when relatively low pressures are used in combination with high anode voltages.

11837-1

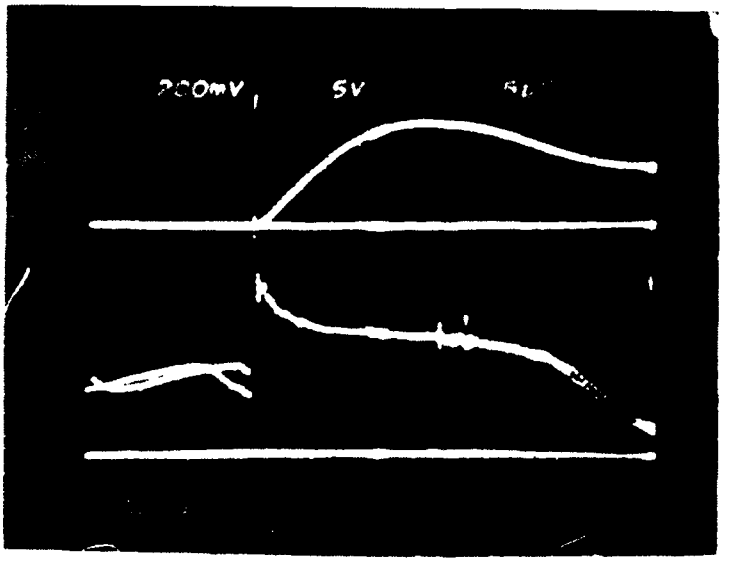

I_S, 500 A/DIV

V_S, 200 V/DIV

TIME, 5 μs/DIV

Figure 14. Source grid current and voltage, P = 0.0368 Torr He.

B. CONTROL GRID CIRCUITRY

The CG intercepts approximately 3 to 5% of the source grid current, I_S, as leakage current when V_{CG} is near cathode potential. The leakage current is also delayed about 4 μs with respect to I_S. This leakage can be significant and the control grid bias circuit must be able to drain it without interfering with the trigger pulse waveform; if not, V_{CG} drifts upwards and the anode begins to switch on prematurely.

In order to keep V_{CG} near the cathode potential, we added additional circuitry which tapped off 5% of the source current and diverted it to the CG. By keeping the relative impedance of this connection high, the trigger pulse waveform is not overly damped.

The CG was originally high-potted to over 5 kV without arcing, and the 10-kV Marx trigger pulser was terminated with a 50-Ω resistor without incident. It was later discovered that the inductance of the termination resistor allowed higher voltages than anticipated to be present and the CG was shorted out by spurious arcing at 6 kV. This arcing problem was eliminated by: replacing the insulating washers and sleeves at the bolt rings (see Figure 2) with single-piece teflon bushings, adding Paschen breakdown protection in the vacuum pump isolator (seen near the right center of Figure 13), and installing a protecting sparkgap set at a safe level which was clearly visible to the operator.

The normal trigger pulse into the CG produced a 400-A current with a 10-ns rise time. Higher currents were generated using a 3-Ω pulse forming network with a 50-ns rise time and a low voltage 1-Ω water line having a 30-ns rise time.

C. ANODE LEAKAGE

The ratio of the anode leakage current to the CG leakage current (3%) is of the same order of magnitude as the ratio of the CG leakage to the source current, as long as $V_{CG} < 0$. Care was taken, as noted above, to maintain V_{CG} as near to cathode potential as was practical in order to avoid serious losses during pulse charging of the anode. While parametric data are not available, it is known, for example, that a charging voltage loss of 5 kV may be expected if V_{CG} exceeds about +30 V. Since this mechanism can have positive feedback, higher leakage currents will tend to run away i.e., cause full anode conduction. To first order, the leakage charge is independent of the anode voltage.

D. SPONTANEOUS (ARC-TRIGGERED) DISCHARGE

Figure 15 shows I_S and V_{CG} for a typical event where one section is operated above the glow-to-arc limit. After 10 μs, I_S has risen to a peak of 1250 A and an arc occurs between SG and CG. This arc does not affect I_S directly since the CG impedance is high. At a random time later, the SG may also arc to the cathode. In Figure 15, the SG-to-cathode arc occurs 3 μs later; the plasma potential (to which the CG has risen) collapses and I_S rises to a higher level.

The rise of V_{CG} caused by a glow-to-arc transition is relatively slow. While the anode is triggered into conduction, the process builds up I_A in a characteristic fashion. The spontaneously triggered load current I_L ($\approx I_A/2$) is seen in Figure 16 on a 50 ns/cm time scale with the BL charged to V_o ~10 kV. The current rises for over 100 ns before the BL charge is dissipated and the current falls off. The center 5-95% portion of the rise fits an exponential curve to about 5%. Nearly the same pulse shape is found if the CG trigger pulse has a rise time longer than 0.1 μs. The rate of rise of I_L is determined in these two cases by the pressure and I_S.

E. TRIGGERED PULSE SHAPE

1. Amplifier-Interrupter Mode

In this subsection we discuss the results obtained when the BL was connected between the anode and the CG as shown in Figure 5a. The functional result of attempting to switch in the amplifier mode is a partial discharge of the BL voltage associated with a fixed charge transfer through the load. The data obtained with one source section show that there is no obvious avalanche build-up of current in the anode section following an initial step function current pulse. Instead, the anode current tracks the CG voltage (at low current) and the CG current as a 1:1 current amplifier (at high current). This amplification is independent of the anode voltage over a wide range. Figure 17 shows I_{CG} and I_A with two different control grid pulse waveforms. (The 50 ns periodic structure on the pulse is an artifact of the pulser and is not directly related to the BL.) Evidently there is no feedback mechanism to supply current between the CG and the SG other than that imposed externally by the trigger pulser. In order to achieve higher anode currents in this mode, it is necessary to drive the control grid with the same current and rise time. We were able to reach I_A ~1 kA by driving the CG harder using low impedance pulsers.

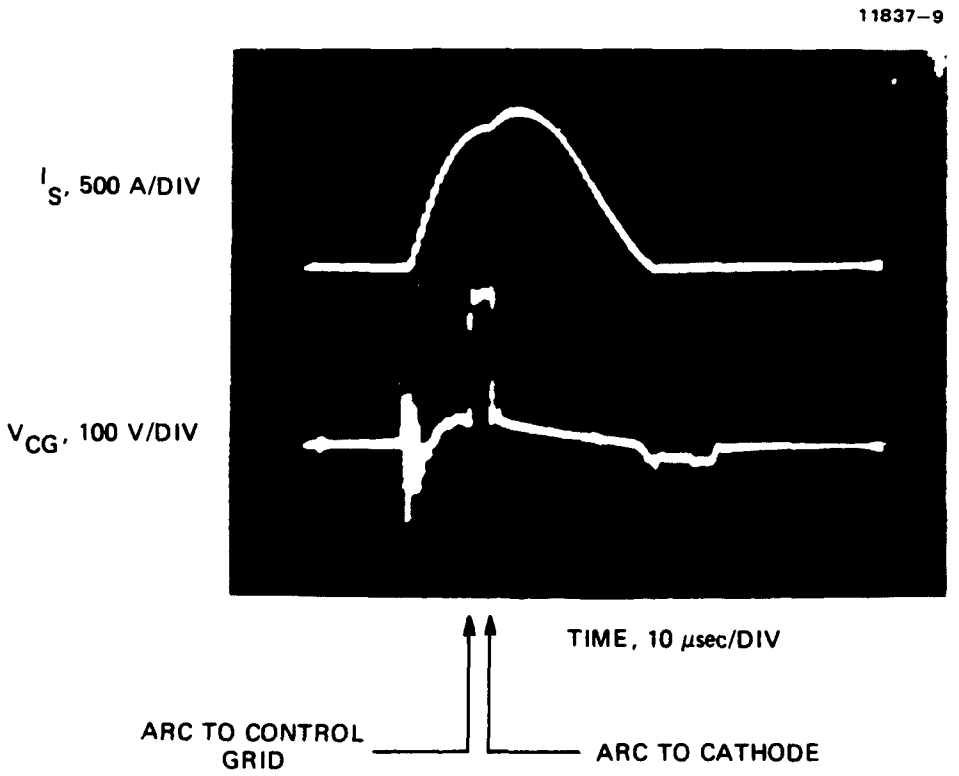

Figure 15. Source current arc limit. The control grid voltage is seen to jump spontaneously up to the plasma potential due to an arc to the source grid after about 10 μs (at $I_S \sim 1250$ A). The control grid voltage collapses later when a second arc shorts-out the source grid to the cathode. Either type of arc will spontaneously switch-on the anode current.

11837-8

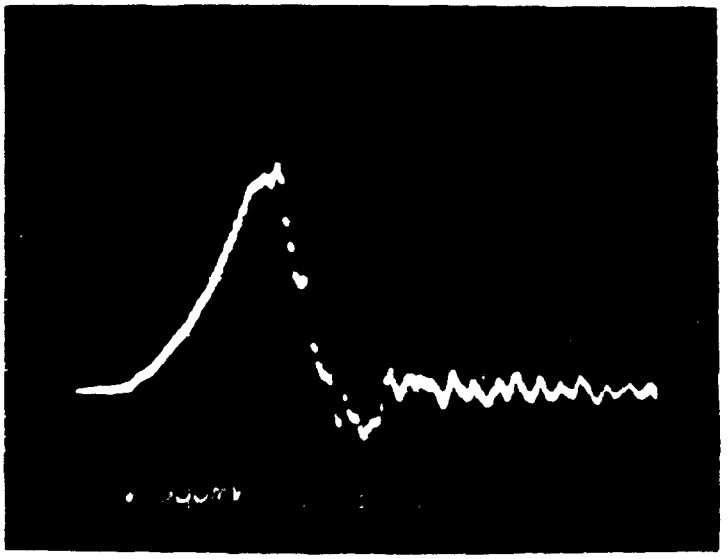

Figure 16. Spontaneously (slow control grid) triggered switch current rise. P = 0.0369 Torr He, I_S = 1100 A. Shows characteristic exponential rise with no sharp leading edge.

11837-7

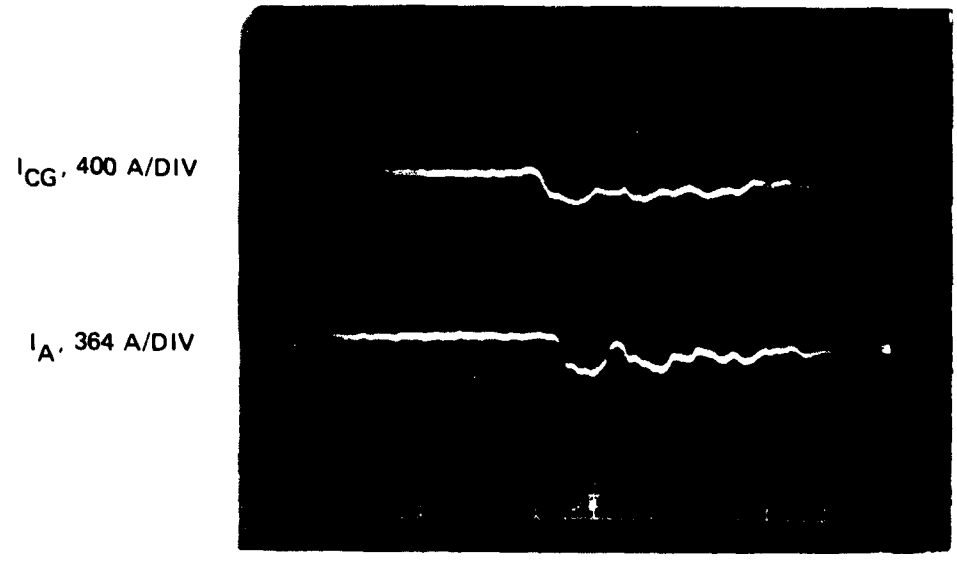

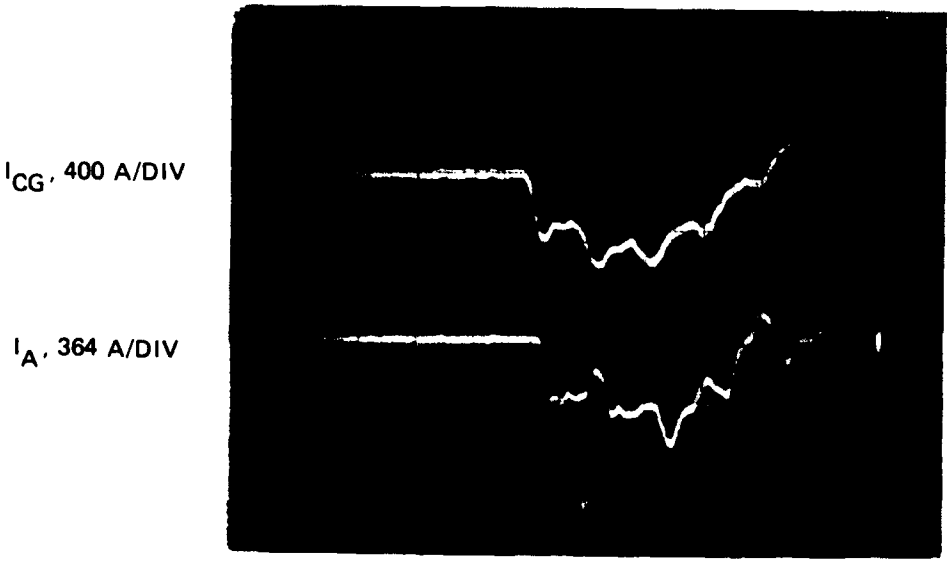

Figure 17. Amplifier mode with two different control grid pulse shapes. P = 0.063 Torr He, $V_o \sim 40$ kV.

2. Feedback Mode — Low V_{CG}

In this subsection we discuss a rearrangement of the BL connections to the switch that provides positive feedback and closing switch operation. In order to supply the full anode current, it is necessary to supply a high current between the control grid and the source grid. To accomplish this, the BL was connected between the anode and the cathode as shown in Figure 5(b). Here, the intent was to feedback the anode current through the other electrodes and have it add to the original trigger pulse. In this case, we find that the anode current is able to rise above the external I_{CG} and cascade to a full discharge condition.

As in the amplifier mode, the rapid anode current phase can be controlled by the CG pulse. For low V_{CG} the rise of the anode current follows V_{CG}. Driving V_{CG} negative interrupts I_A. Multiple low current pulses have been generated in this fashion. Once V_{CG} approaches V_S this control feature is lost and feedback from the anode current locks the switch into the on state.

3. Feedback Mode — High V_{CG}

For higher CG drives ($V_{CG} > V_S$) the load current pulse waveform is found to be essentially of fixed shape and scales linearly with V_o over a wide voltage range. The roughly linear scaling of the current pulse is shown in Figure 18(a) and (b) where the signals were obtained at V_o = 3.7 and 7.7 kV and recorded at different amplifications. The first rapid rise in the signal is (within experimental error) consistent with space charge limited electron flow. The anode voltage and current are related through Child's Law by

$$I_A = A_o\, kV_A^{3/2}/d^2 \quad , \qquad (1)$$

11837-6

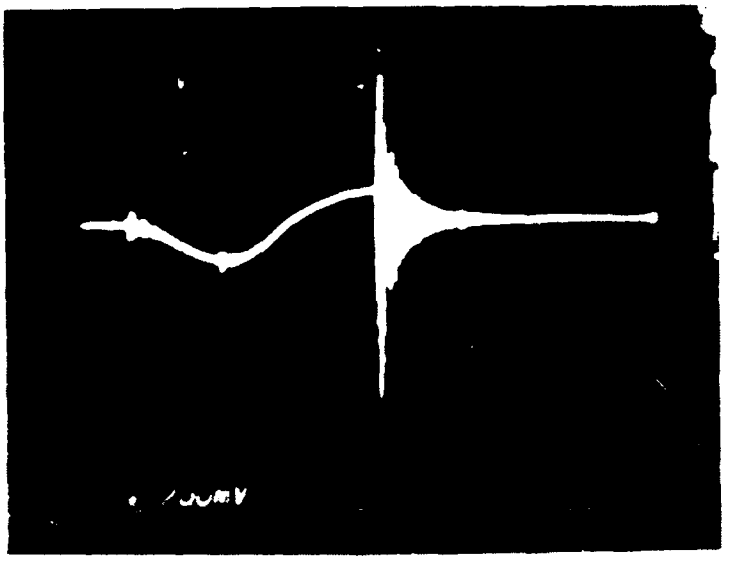

ANODE VOLTAGE, 6.8 kV/DIV

TIME, 5 μsec/DIV

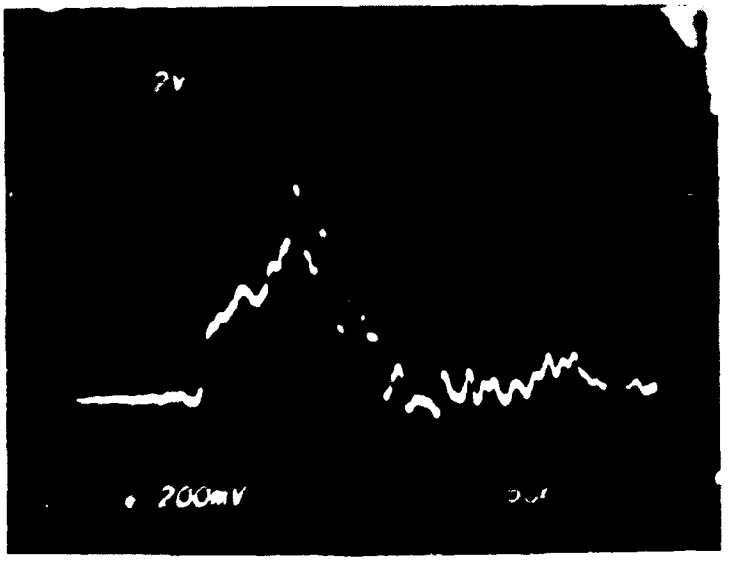

ANODE CURRENT, 146 A/DIV

TIME, 50 nsec/DIV

(a)

Figure 18. Voltage effect on anode pulse. I_S + *)) A, P = 0.0362 Torr He. (a) V_o = 3.7 kV, (b) V_o = 7.7 kV. Peak currents are in the ratio 3.7/7.7.

11837-5

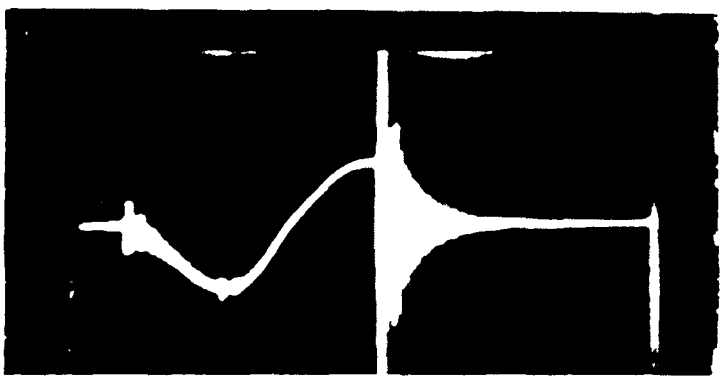

ANODE VOLTAGE, 6.8 kV/DIV

TIME 5 μs/DIV

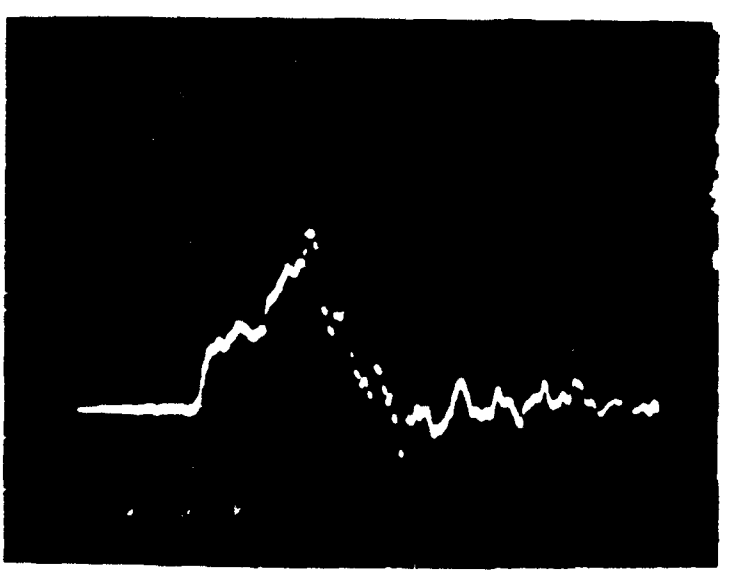

ANODE CURRENT, 364 A/DIV

TIME, 50 ns/DIV

(b)

Figure 18. Continued.

where A is the effective area, d is the spacing, and $k = 2.33 \times 10^{-6}$ in MKS units. The current and voltage must also obey the load-line characteristics of the BL network that is, instantaneously

$$R_{1/2} I_A + V_A = V_o \qquad (2)$$

where $R_{1/2}$ is the impedance of one half of the network and V_o is the initial network voltage. The space charge limited anode current I_1 must initially satisfy both of these criteria. The effective area for electron emission that is required to match the data is $A_o = 1100$ cm^2, or a band slightly smaller than the total width of the active cathode section. This rough fit to the data is shown in Figure 19. Since the source plasma density is expected to be considerably more localized than the above area, some change in the effective area must be expected as the anode current is increased due to saturation starting at the outer edges where the plasma density is low and moving in as the current increases. This behavior is similar to the saturated emission characteristics of thermionic vacuum diodes.

The second phase of the anode current rise is qualitatively identical to the spontaneously triggered case. Although it starts off from a finite level, it follows the same exponential rise until the BL charge is depleted. The exponential growth rate Γ increases with pressure and source current. Figure 20 shows the increase in the growth rate with pressure for a fixed anode voltage (7.5 kV) and source current (880 A). Only for the higher pressures does the anode current rise fast enough for the switch to fully close and begin to show a flat top within the 50 ns pulse width of the BL. The linear dependence on P is shown explicity in Figure 21. High pressures are not compatible with high voltage operation. Paschen breakdown imposes a limit of 35-40 mTorr on the switch pressure due to the 4 cm spacing along the insulators. Consequently, we examined high source currents as an alternative approach.

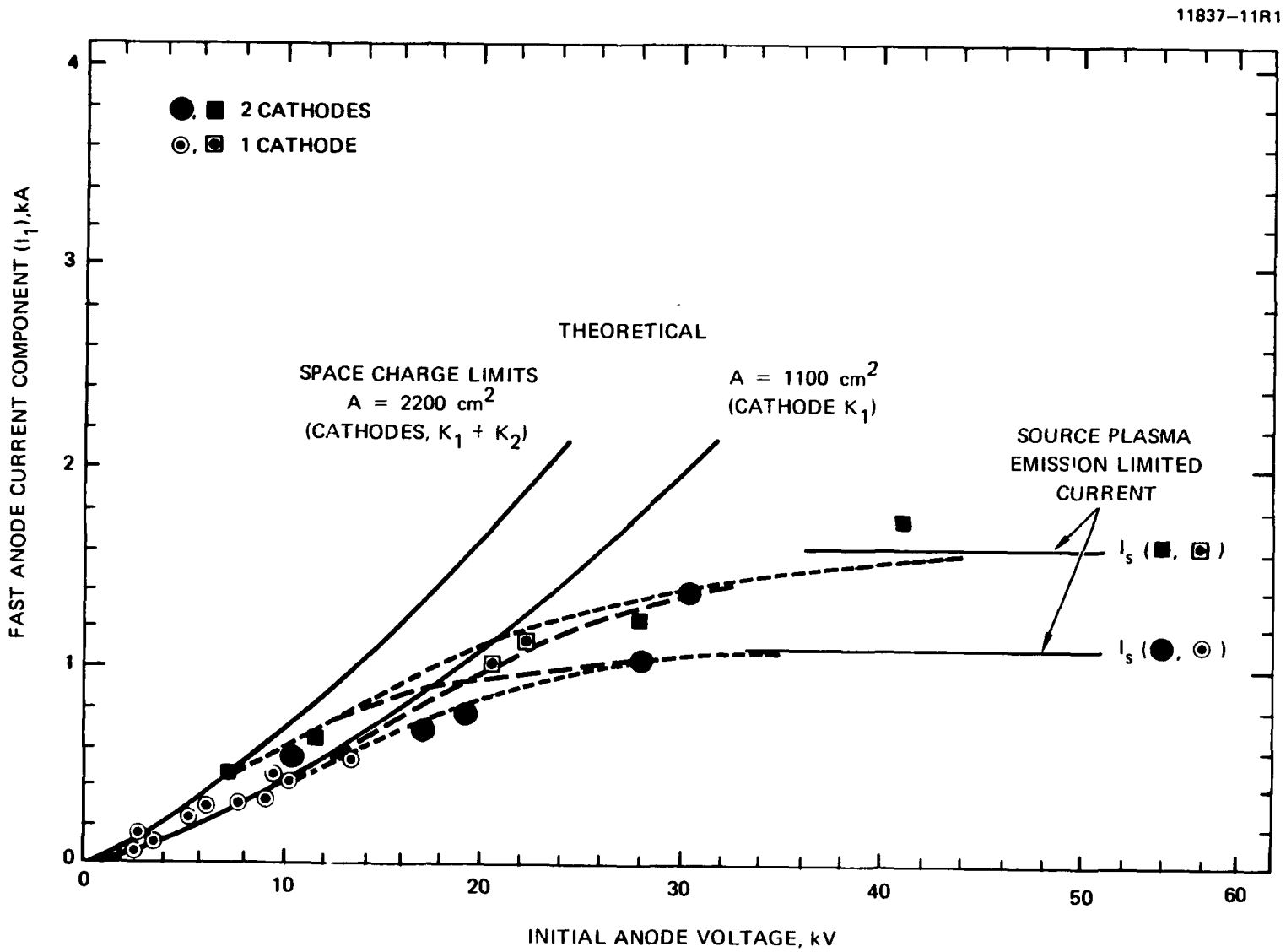

Figure 19. Saturation characteristics of the fast anode current component I_1 due to space charge limited electron current. For low anode voltages, I_1 is limited by space-charge effects. For high anode voltages I_1 is limited by source plasma emission. The source emission limits appear to be independent of area (i.e., whether the emission comes from one or two cathodes).

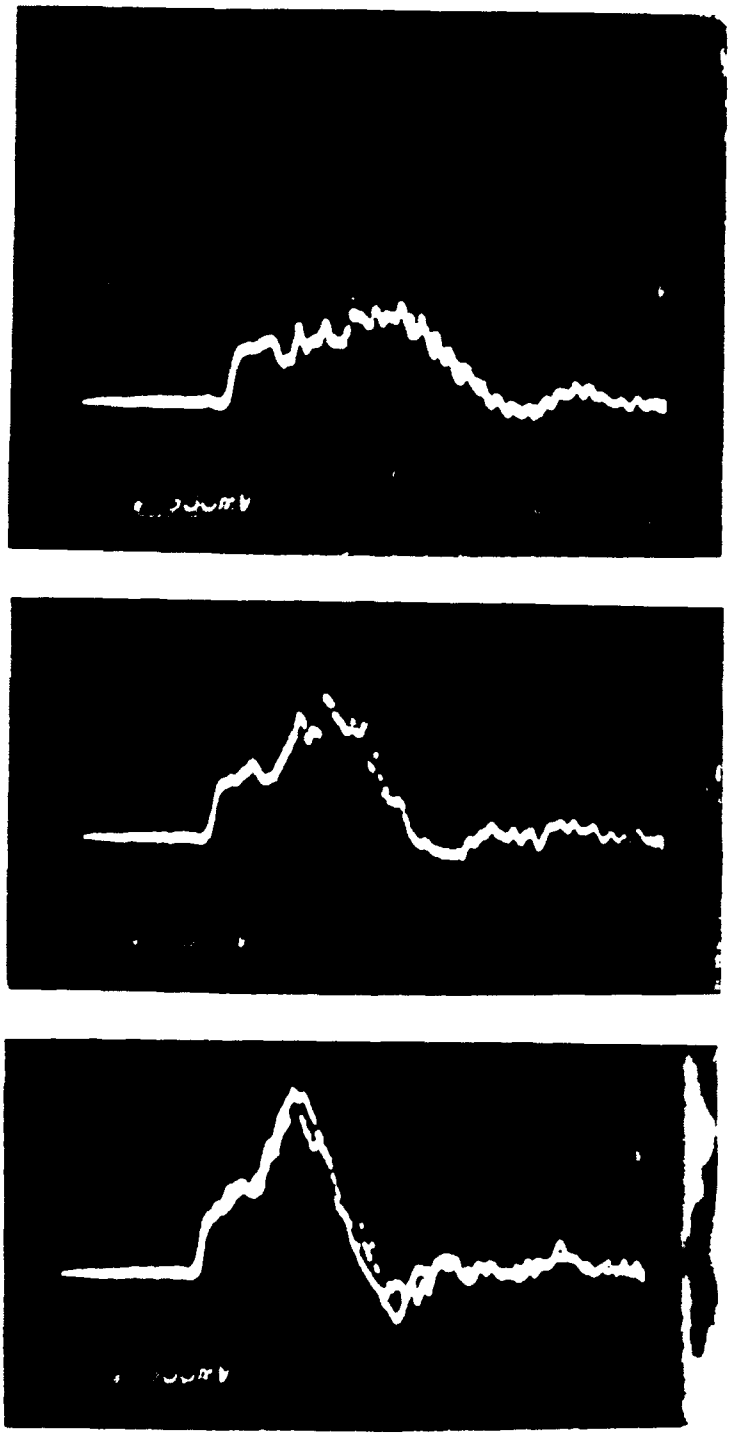

Figure 20. Anode current growth increase with pressure.
I_S = 880 A, V_o = 7.5 kV

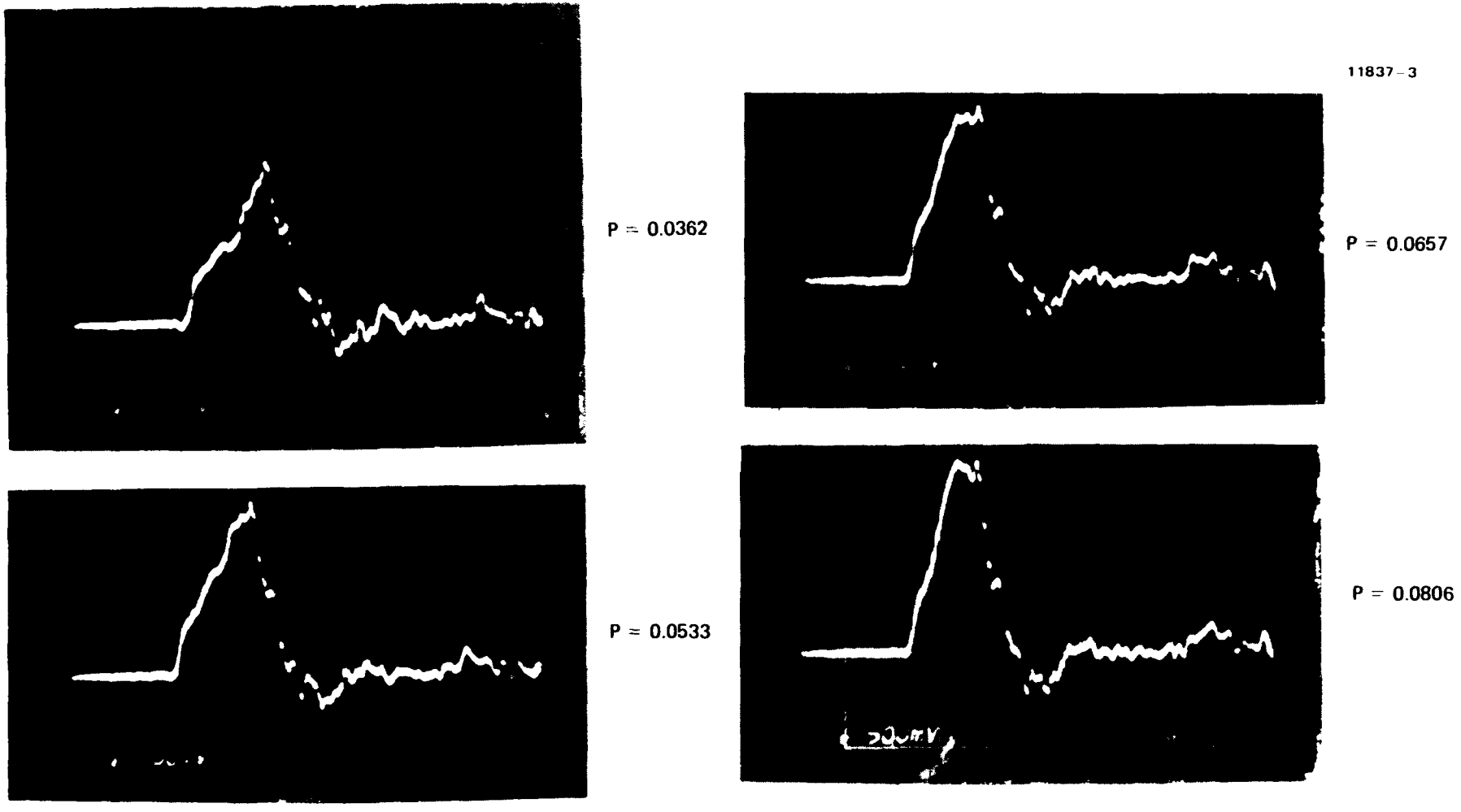

Figure 20. Continued.

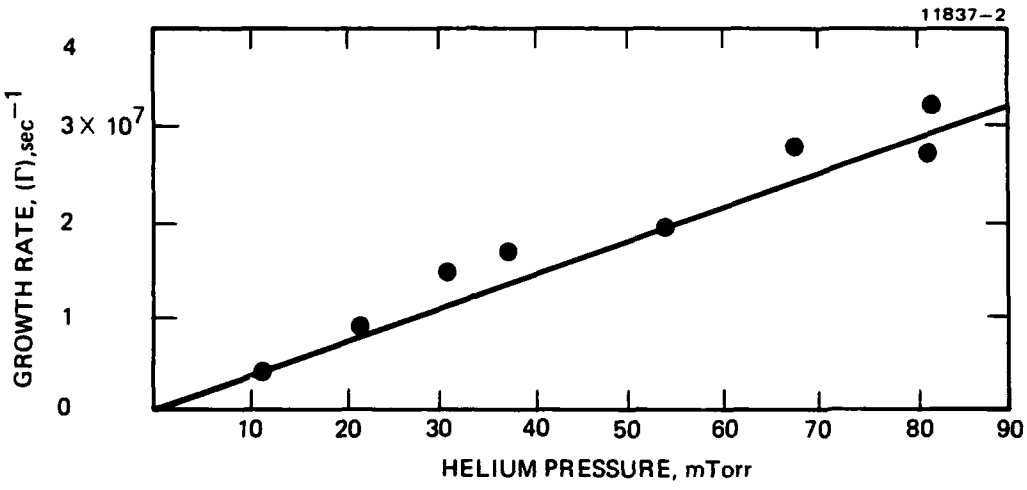

Figure 21. Anode current growth rate increase with pressure. I_S = 880 A, V_o = 7.5 kV.

4. Source Current I_S Enhancement of the Growth Rate of I_A

The source current density affects the growth rate in much the same way as pressure does. Only the source current I_S from each of the two cathodes can be measured in our equipment. Therefore, we take I_S as a measure of the current density. Figure 22 shows a sequence of pulses generated with the same voltage as above and a pressure of 37 mTorr. For low I_S (below I_1), the rapid current rise is damped and may even decay back down following the initial impulse. As I_S increases the growth rate changes from a negative to a positive sign and a linear increase of Γ with I_S is observed. These results were obtained with I_{CG} = 400 A. To some extent higher I_{CG} pulses can be used to accommodate low I_S currents, with the growth rate reaching near to a limit imposed by the larger of I_S or I_{CG}.

If I_S, I_{CG}, and P are fixed, the growth rate decreases essentially inversely with V_A. A cutoff (Γ = 0) occurs when I_S is exceeded by the space charge limit I_1. This is attributed, in part, to the initial source plasma being unable to supply enough current to hold the plasma potential below the crossed field discharge limit in the source section as the anode current rises. Once this condition prevails, the feedback mechanism is ineffective.

5. Multiple Cathodes

The effect of the area or the number of parallel source sections was investigated by adding magnets to the second cathode section, K_2. The discharge voltage of K_2 was found to be 50 V lower relative to K_1. In order to reach higher net source currents, we added a small resistance and inductance into one cathode lead and were able to adjust the two source currents to within about 10% of each other and condition the current in the glow discharge to 1800 A. The switch was originally designed to have the control grid grounded to the BL via a low inductance path. Since the upper cathode needed to be grounded instead, (and the lower cathode floated with respect to it) we attempted to supply a low inductance ac path between the cathodes by using four 0.1-μF extended foil capacitors. The lower limit of the response of this ac shunt at high frequency is indicated by an observed resonance at $\omega \sim 4 \times 10^6$ sec^{-1}. The higher measured growth rates discussed below may be underestimates of that obtainable with a more ideal arrangement.

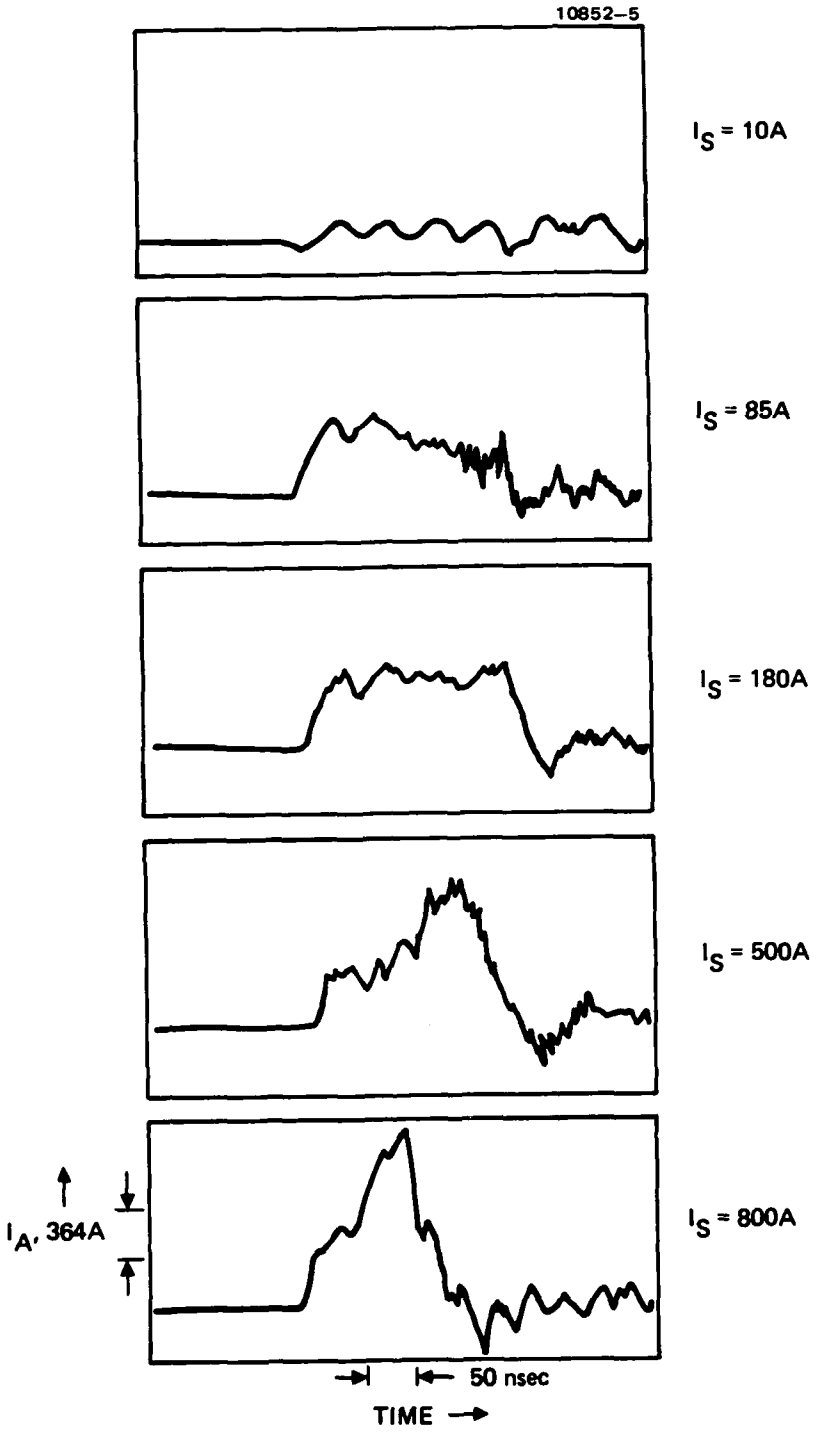

Figure 22. Effect of source current on anode current rise. P = 0.0370 Torr, V_o = 7.3 kV.

The data obtained with two cathode sections are similar to those obtained with a single cathode. However, the space charge limit did not double at higher voltages as seen in Figure 19. This may have been partly due to saturation effects and partly due to the finite response time of the shunt capacitors. Growth rates are discussed in the next section.

F. GROWTH RATE DEPENDENCE

The growth rates were measured at a pressure P_o = 33-37 mTorr for a variety of conditions (with anode voltages of 7-40 kV and source currents of 85-1800 A). These are plotted in Figure 23 as a function of I_S/NI_o, where N is the number of cathode sections. The linear dependence of Γ is evident. The zero intercept occurs near $I_S = I_1$ so we may write

$$\Gamma \approx \frac{P}{P_o}\frac{A_o}{A}\left(\frac{I_S - I_1}{I_o}\right)\Gamma_o = \frac{P}{P_o}\left(\frac{J_S - J_1}{J_o}\right)\Gamma_o \qquad (3)$$

where $\Gamma_o \sim 3.4 \times 10^7$ sec^{-1}, P_o = 33 mTorr, $J_S = I_S/A$, $J_1 = I_1/A$, and $J_o = I_o/A_o$.

This gives an anode current dependence of the form

$$I_A = I_1 \exp\left[\frac{P}{P_o}\left(\frac{J_S - J_1}{J_o}\right)\Gamma_o t\right] \quad . \qquad (4)$$

The net predicted switching time for which $I_A = I_o$ is given by

$$\Delta t = \frac{P_o}{\Gamma_o P}\left(\frac{J_o}{J_S - J_1}\right) \ell n \ \frac{J_o}{J_1} \quad . \qquad (5)$$

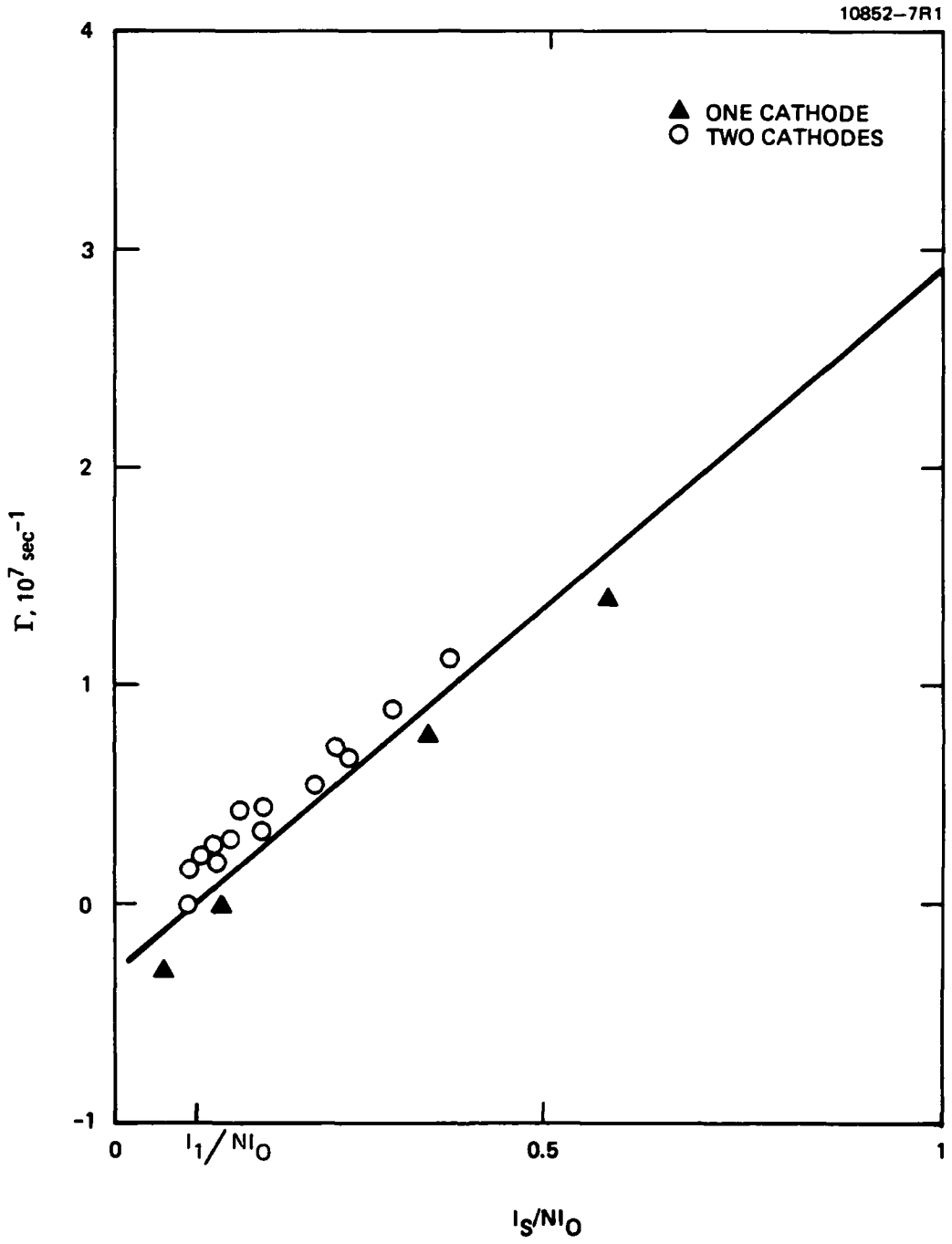

Figure 23. Growth rate data distribution. Shows linear dependence on the source current, inverse dependence on number of cathode sections and Blumlein short circuit current.

SECTION 4

THEORETICAL MODELS

A. COLLECTIVE ACCELERATION MODEL

The model which we previously developed[3] assumes a half-space plasma with a sharp boundary held in place by an external grid electrode. When the grid is removed (i.e., biased positive), the plasma is free to expand. Two aspects of this expansion are important. First, the thermal-electron pressure develops a space-charge separation at the boundary such that the electrostatic field balances the kinetic pressure of the electrons. This field also acts on the ions and can accelerate them to energies in excess of their thermal energy. Eventually, this mechanism would cool the electrons and accelerate the ions leading to ambipolar diffusion where the expansion velocities of the two species are nearly equal (i.e., $v_e = v_i = \sqrt{2kT_e/M_i}$). If the higher energy electrons are continually replaced by some external mechanism, then this cooling does not need to take place, and ions near the boundary can obtain velocities in excess of $v_i = \sqrt{2kT_e/M_i}$. Second, the initial shape of the boundary determines how many ions are exposed to the high electric field of the sheath and the intensity of the field itself. Consequently, the transient startup conditions can lead to a variety of results. These range from conventional ambipolar diffusion, when the boundary is diffuse or the electrons cool rapidly, to the accelertion of a small number of ions to speeds an order of magnitude larger than the ambipolar case. This latter result is of interest to the switching problem. In the following analysis, we presume that high temperature electrons are regenerated in the source section and that the initial plasma boundary is sharp.

The results obtained under the previous study contract presumed a constant anode voltage. Here we use a voltage which is consistent with that of a pulse forming network with impedance R, i.e., $V = V_o - IR$, where I is the switch current and V_o the initial voltage. The space charge limited current is then replaced in Reference 3 by

$$J \sim K\,(V_o - IR)^{3/2}/(d - \sqrt{kT_e/M_i}\cdot(2+\ln(J_o/J))\cdot t)^2 \quad , \qquad (6)$$

where $K = 2.3 \times 10^{-6}$, d is the boundary to anode spacing, and J_o is the total electron flux from the source in the forward direction, ($J_o = en_o \sqrt{kT_e 2\pi m_e}$). Equation 6 incorporates a drift velocity which differs from the purely ambipolar case through the logarithm term. The latter arises due to extraction of electrons by the applied external field. The current density is nonlinear in J but may be inverted and solved for time as a function of the current. After replacing J by the equivalent current we can solve for t:

$$t = d\sqrt{\frac{M_i}{kT_e}}\left(\frac{1-\sqrt{\frac{KV_o^{3/2}}{I}\frac{A}{d^2}\left(1-\frac{RI}{V_o}\right)^{3/2}}}{2+\ell n\ \frac{I_s}{I}\sqrt{\frac{M_i T_e}{m_e T_i}}}\right) , \qquad (7)$$

where I_s is the source current. The current reaches the maximum level V_o/R at a finite time given by

$$t = d\sqrt{\frac{M_i}{kT_e}}\left(\frac{1}{2+\ell n\left(\frac{I_s}{I}\sqrt{\frac{M_i T_e}{m_e T_i}}\right)}\right) . \qquad (8)$$

At t = 0, the initial space charge limited current is a solution of the cubic equation,

$$I_1 = \frac{KV_o^{3/2}}{d^2}A\left(1-\frac{RI_1}{V_o}\right)^{3/2} . \qquad (9)$$

Typically, this results in a characteristic pulse waveform (Figure 24) having an initial step rising to I_1 in an electron transit time followed by a roughly exponential rise to the maximum of the PFN. Inductance would characteristically delay the rise, but the characteristic knee would still be apparent.

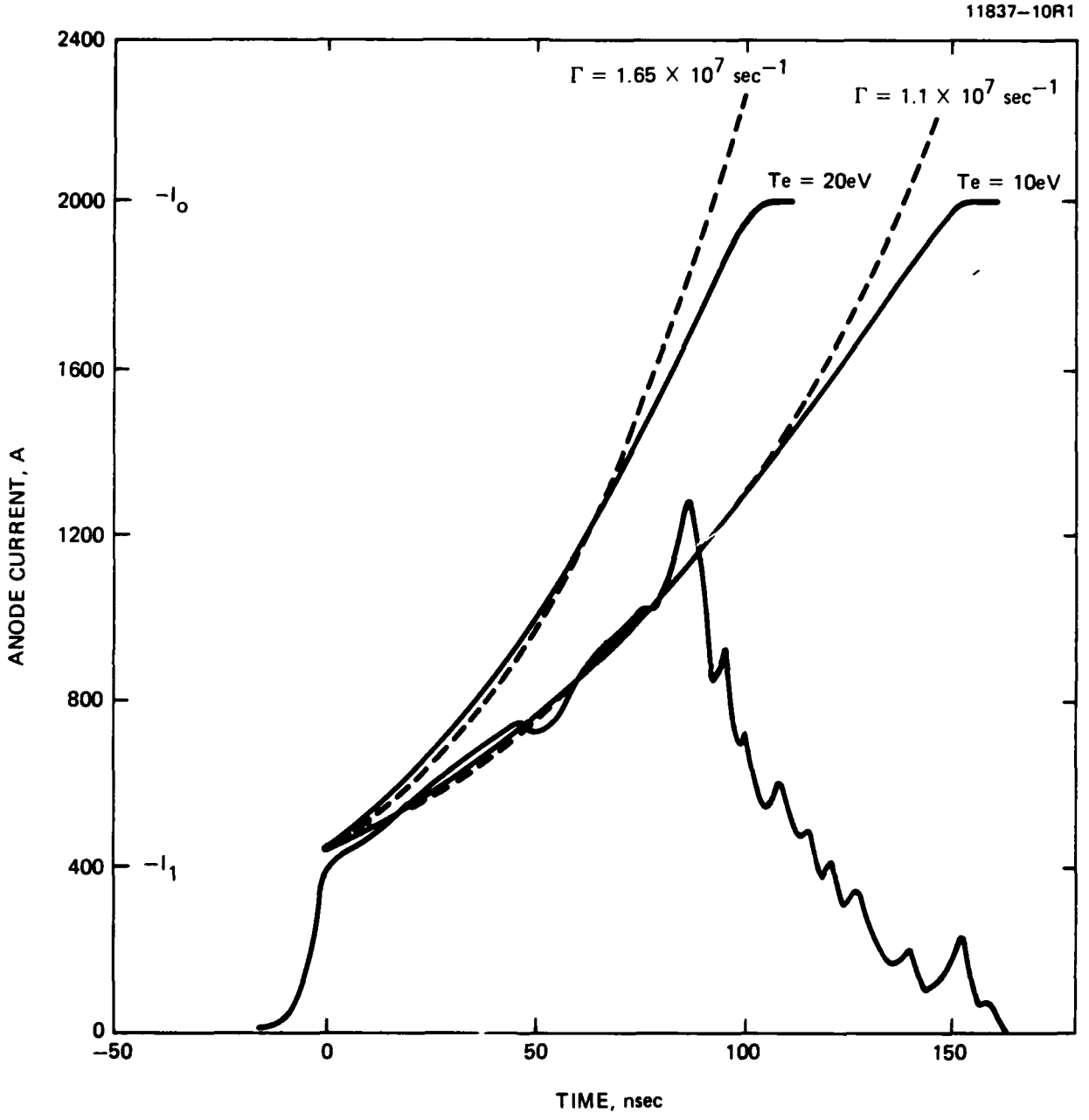

Figure 24. Comparison of experimental pulse shape with collective acceleration (solid curve) and exponential (dashed) models.
[I_S = 880 A, V_o = 10 kV, A = 0.11 m^2, P = 33 mTorr He, and T_i = 0.05 eV]

The example shown assumes several Maxwellian electron temperatures. This was done in order to match the actual distribution function in a crossed field discharge (which is non-Maxwellian, having a low temperature core and a high temperature tail extending to hundreds of volts). The high energy electrons in the tail are continually regenerated at the cathode. The analysis has not taken into account the geometrical effects of a real grid electrode upon the initial phase space distribution functions near the initial boundary. As a minimum, in order for the model to be valid, the grid pulse rise time would have to be a few nanoseconds or less.

B. COMPARISON OF THEORY WITH EXPERIMENTAL RESULTS

The observed increase of Γ with I_S was anticipated qualitatively. However, the model is not strictly valid unless $I_S \gtrsim I_o$ and rapid switching times were not expected unless the electron temperature $\gg$ 10 eV. A minimum was also expected in the pressure dependence of Γ; at high pressure ionization in the gap would dominate, while at low pressure the source discharge voltage would increase causing the temperature to rise. Such a minimum in Γ was not found. The collective acceleration model is consistent (within the experimental errors) to an exponential growth of current following a sharp rise. This is shown in Figure 24 were a comparison of the model is made with a simple exponential growth law and a typical pulse waveform at V_A = 10 kV. It should be noted that the collective model does not exhibit a strong I_S dependence and is not strictly valid for $I_S < I_A$.

The area dependence implies that current density, rather than gross current determines the source induced growth mechanism. Consequently, it is desirable to operate the device at as high a source current as possible in a single section rather than multiple sections used in parallel. Using these data to scale the time required to fully close the switch yields 28 ns at I_S/I_o = 1.5 using a predicted Γ of 3×10^7 sec^{-1} and a pressure P > 33 mTorr.

SECTION 5

CONCLUSIONS

The anode current growth in a Crossatron switch has been shown to be controlled by several parameters. In order to achieve the desired switching behavior at high peak powers, it will be necessary to substantially increase the source current density without arcing. If the ratio of the source current to the short circuited anode current exceeds about 1.5, then the present empirical data predict a total time to full closure of about 23 ns. This closure takes place in two steps. The first is an abrupt rise due to space charge limited electron flow. The second step is an exponential growth due to a combination of pressure dominated collisional processes and source current enhanced breakdown. It is not clear if the last mechanism actually involves collective acceleration processes, but the net effect is qualitatively the same as predicted theoretically.

In order to demonstrate the validity of the scaling of the growth rate with $I_A > 2$ kA, it will be necessary to substantially increase the glow-to-arc limit in the source section to enable higher source current density. As a first step, this will require: sealing the surface of the fiberglass insulators to eliminate dust, electro-polishing the cathodes, chemically cleaning the switch assembly, and (following reassembly) a few thousand pulses at high current to current-condition it. Ultimately, good engineering practice would dictate the use of bakeable ceramic to metal seals instead of O-rings and plastic insulators.

ACKNOWLEDGEMENTS

Mr. Hayden Gallagher collaborated in engineering and testing the crossatron. Mr. Roland Fleig, Mr. Allan Kramer and Mr. James Rose provided technical support during this program.

REFERENCES

1. R. J. Harvey, M. A. Lutz, H. E. Gallagher, "Current Interruption at Powers up to 1 GW with Crossed Field Tubes," IEEE Plasma Sci., Vol 6, No. 3, Sept. 1978.

2. R. E. Hester, et al, UCRL - Preprint 82448, "The Experimental Test Accelerator (ETA)," March 1979; and
   E. Cook, L. Regimato, "Off Resonance Transformer Charging for 250-kV Water Blumlein," IEEE 1978 13th Pulse Power Modulator Symposium.

3. R. Harvey, H. Gallagher, and S. Hansen, "Pulse Power Switch Development," Final Report HRL, Oct. 1980 (N60921-79-C-0271)